Early Archean (ca. 3.5 Ga) microfossils and ^{13}C-depleted carbonaceous matter in the North Pole area, Western Australia: Field occurrence and geochemistry

Yuichiro UENO[1]*, Shigenori MARUYAMA[1], Yukio ISOZAKI[2], and Hisayoshi YURIMOTO[1]

1: *Department of Earth and Planetary Sciences, Tokyo Institute of Technology, Tokyo 152-8551 Japan*

2: *Department of Earth Science and Astronomy, University of Tokyo, Meguro, Tokyo 153-8902, Japan*

Corresponding author, e-mial: ichiro@geo.titech.ac.jp, Fax: +81-3-5734-3538

Abstract

Microfossils and ^{13}C-depleted carbonaceous matter in ~3.5 Ga North Pole area, Pilbara craton, Western Australia, are investigated. Carbonaceous filamentous microstructures, which represent previously known taxa of Archean microfossils, were found in a new locality of bedded chert in the North Pole chert-barite unit. $\delta^{13}C$ values of carbonaceous matter from the same fossil-bearing chert vary from –40 to –31 ‰, suggesting a biological origin of the carbonaceous matter. The large fractionation up to –40 ‰ could have been produced by autotrophs utilizing the Calvin cycle or reductive acetyl-CoA pathway, but not by cyanobacteria. Detailed study on geology, sedimentology and petrology of the fossil-bearing chert/barite beds provided the following new lines of evidence: (1) the fossil-bearing chert/barite beds are mainly composed of fine-grained silica and partly barite with or without mafic clastics and lack quartzo-feldspathic coarse-grained clastics; (2) they show parallel lamination, partly massive, and lack cross-lamination; (3) several generations of silica and barite veins cut the chert/barite beds and some of them were depositionally overlain by fossil-bearing chert. These observations suggest that the fossil-bearing chert was deposited sufficiently distant from a landmass and probably well below wave base. Moreover, the cross-cutting relationships between beds and veins suggest that deposition of the fossil-bearing chert/barite beds was synchronous with hydrothermal activity. Further, a huge amount of ^{13}C-depleted carbonaceous matter is concentrated in the silica dikes, which filled extensional fractures below the chert-barite unit. Based on these observations, we suggest that the seafloor hydrothermal system including the sub-seafloor was the habitat of the Early Archean life. The Early Archean mi-

crobial community in the hydrothermal system was probably supported by chemosynthetic primary producers.

1. Introduction

In recent decades, Earth's early biosphere has become a major interest of paleobiological research. Understanding of the earliest ecosystems during the first 1 billion years of Earth's history mainly comes from microfossil records (e.g., Awramik et al., 1983; Schopf, 1993) and carbon isotopic distributions of sedimentary organic matter (e.g., Hayes et al., 1983; Mojzsis et al., 1996; Schidlowski, 2001). The oldest known microfossils (ca. 3.5 Ga) include trichomic cyanobacteria-like forms suggesting that oxygenic photoautotrophs may have existed already in the Early Archean (Schopf, 1993). Isotopic analyses of the Early Archean sedimentary organic carbon revealed that autotrophic organisms had already appeared on Earth at least by 3.5 Ga (Hayes et al., 1983; Schidlowski, 2001) and probably by 3.8 Ga (Mojzsis et al., 1996; Ueno et al., 2002).

Independent from the geological record, biologists have recently discovered microorganisms in extreme environments such as high temperatures over 100°C, low pH, and high salinity (e.g., Stetter, 1998). The discovery has enlarged knowledge of the modern biosphere and made the existence of extraterrestrial life more plausible. The remarkable progress in microbiology has also required re-evaluation of Earth's earliest biosphere.

The oldest morphologically preserved microfossils (Awramik et al., 1983; Schopf, 1993; Ueno et al., 2001) occur in sedimentary rocks in the ca. 3.5 Ga North Pole – Marble Bar area in the Pilbara Craton, Western Australia. The area is one of the best candidates for the study of the Early Archean biogeochemical record, because of its low metamorphic grade (prehnite-pumpelleyite to lowermost greenschist facies; Buick and Dunlop, 1990). However, detailed stratigraphy of the fossil-bearing horizons and regional distribution of the microfossils are still poorly known.

Pioneering work on fossil-bearing sedimentary rocks from the North Pole area (Buick and Dunlop, 1990) indicated that they were originally deposited in a shallow marine evaporitic setting based on the occurrence of replaced evaporitic gypsum, stromatolite-like structure and silicified cross-laminated sandstone. However, recent field work (Isozaki et al., 1997, 1998; Nijman et al., 1999; Ueno et al., 2001) suggested that the hydrothermal activity was synchronous with the deposition of the fossil-bearing sedimentary rocks. Furthermore, recent study on hydrothermal alteration of the fossil-bearing rocks and related basaltic volcanics (Kitajima et al., 2001) suggested that they were probably deposited in deep water below 1500 m. Thus, re-evaluation of fossil-bearing sedimentary rocks is needed for deducing the habitat of Early Archean organisms.

In order to re-evaluate the depositional environment of the fossil-bearing sedimentary rocks, intensive field mapping and rock sampling were carried out in the North Pole area in 10 field seasons during the period 1991-2001. In this study, more than 600 rock specimens were scanned for microfossil research. As a result, we identified carbonaceous filamentous microstructures with ^{13}C-depleted isotopic compositions from a new locality of bedded chert. We carried out 1/5000-scale mapping around the fossil locality as well as 1/100 and 1/50-scale detailed sketch of the fossil outcrop. In order to study the distribution of microfossils, we examined about 200 thin sections from the fossil outcrop.

In this paper, we report (1) detailed geology, stratigraphy and petrography of the fossil-bearing chert bed, (2) morphotypes of the newly-found carbonaceous filaments, and (3) their carbon isotopic signature. We will re-evaluate the depositional environment of the fossil-bearing chert bed and discuss the physiological aspects of Early Archean microfossils.

2. Geological outline of the North Pole area

The North Pole area in the Pilbara craton, the locality of the oldest microfossils (Awramik et al., 1983; Ueno et al., 2001), is located nearly 160 km south of Port Headland, and nearly 50 km west of Marble Bar. In the North Pole area, the lower part of the Warrawoona Group crops out (van Kranendonk et al., 2001), and consists of ca. 6 km thick basaltic greenstones intercalated with 1 to 70 m thick bedded cherts in three horizons (Fig. 1; Isozaki et al., 1997). Among the three, the lowermost chert unit is unique; it is 1 to 70 m thick and is intercalated with several barite beds of 0.1 to 5 m thick. This chert unit associated with barite corresponds to the "chert-barite unit" previously described by Buick and Dunlop (1990). The other two chert units are thinner (1-13 m) than the chert-barite unit, and scarcely associated with barite.

The precise age of the chert-barite unit has never been dated directly. Zircon U-Pb dating yielded an age of 3458 ± 2 Ma for the felsic volcanics (Thorpe et al., 1992) that overlie the cherts and greenstones in the North Pole area. A model lead age of 3490 Ma (Thorpe et al., 1992) was obtained for galena from the chert-barite unit.

This may represent the actual depositional age of the chert-barite unit.

In the North Pole area, numerous (>2000 identified) silica dikes characteristically intruded into the greenstones (Figs. 1 and 2). They are 0.3-20 m wide and generally >100 m long, with the longest over 1 km. The dikes are massive and are composed mainly of chert-like fine-grained silica (~1 μm). The silica dikes are distinguished from the bedded sedimentary chert by their discordant relationships to adjacent strata and by lack of internal bedding. In addition to the silica dikes, 0.1 to 2 m wide barite veins intruded into basaltic greenstones. In the North Pole area, the distribution of the barite veins is laterally discontinuous and is generally restricted to the uppermost ~300 m of the pillow lava below the chert-barite unit, whereas the silica dikes occur 1000 m below the chert-barite unit. Both the silica dikes and the barite veins intrude into chert beds of the chert-barite unit but do not cut through the entire chert-barite unit, nor into the overlying pillow basalt. The tops of the silica dikes show a gradual transition into certain chert beds, forming a clear T-junction. These relationships suggest the silica dikes were formed intermittently during the deposition of the chert beds of the chert-barite unit (Isozaki et al., 1997, 1998; Nijman et al., 1999; Ueno et al., 2001).

In the North Pole area, morphologically preserved fossil bacteria were previously reported from chert beds (i.e., Locality-A and -B of Awramik et al. (1983)) and silica dikes (i.e., Locality-1 and -2 of Ueno et al. (2001)). Among the four localities, three (Locality B of Awramik et al. (1983) and Locality-1 and -2 of Ueno et al. (2001)) belong stratigraphically to the chert-barite unit and associated silica dikes (Fig. 1). The Locality-A of Awramik et al. (1983) has not yet been re-located (Awramik et al., 1988; Buick, 1984, 1988). Thus, for the present, microfossils in the North Pole area occur only in the chert-barite unit and associated silica dikes, and have not yet been found from the overlying horizons.

3. Fossil-bearing bedded chert (Locality-3)

3.1. General description of Locality-3

Newly-found microfossils occur in the northern part of the North Pole area (Loc.-3: 21° 05‘ 05“ S, 119° 26‘02“ E; Figs. 1 and 2). At the Loc.-3, 3 to 20 m-thick chert/barite beds overlie a ~2000 m-thick altered pillow lava together with more than 100 silica dikes (Fig. 3). These rocks are tectonically separated from the overlying basaltic greenstone by layer-parallel thrusts (Kitajima et al., 2001). Further, the thrusts are cut by a high-angle fault trending NE to SW. Radial high-angle faults from the North Pole Monzogranite (3459±18 Ma; Thorpe et al., 1992) suggest that the fault may have been activated by the doming. In addition, a dolerite dike with a NE to SW trend cuts the entire above-mentioned structures. The dike is over 5 km long and also cuts the North Pole Monzogranite. The trend and cross-cutting relationship suggest that the dolerite dike is comparable to the Late Archean Black Range Dyke (Blake, 1993).

The fossil-outcrop is located on the northwestern side of the high-angle fault (Fig. 2). On this side, the greenstone/chert sequence is tectonically duplicated by layer-parallel thrusts and is separated into nine tectonic slices (slice-1 to slice-9; Fig. 2). Each slice has chert/barite beds on the top with or without underlying altered pillow lava and associated silica dikes and barite veins. The distribution of these slices defines a typical duplex structure and suggests E-W trending layer-parallel shortening. Fig. 3 shows the stratigraphy of the nine tectonic slices. The chert-barite beds of all the slices have comparable stratigraphy and show repeated cycles of a distinctive facies association, which is composed of the following lithotypes, from bottom to top: (1) mafic breccia with a cherty matrix, (2) fining-upward mafic silicified sandstone and mudstone, which is now composed mainly of microcrystalline silica, (3) white, red, black, gray, and brown banded chert, (4) bedded barite intercalated at the upper horizon.

On the other hand, the chert/barite beds on the southeastern side of the high-angle fault are relatively undeformed and can be laterally traced over 15 km (Figs. 1 and 2). The fossil-bearing chert/barite beds are laterally traced for at least 50 m in the continuous outcrop at Loc.-3 (Fig. 4). In spite of the intense deformation of the chert beds, these observations clearly indicate that the fossil-bearing chert belongs to the chert-barite unit.

Around the Loc.-3, abundant barite veins intruded into the pillow lava below the chert-barite unit in connection with silica dikes. Distribution of the barite veins defines a fanning pattern focused at a depo-center nearly 200 m below the bottom horizon of the chert-barite unit (Fig. 3).

3.2. Outcrop of the fossil-bearing chert/barite beds and their detailed stratigraphy

Fig. 5 shows a detailed sketch of the fossil-bearing horizons in one outcrop. The chert/barite bed is 4 m. These horizons are intruded by over ten barite and silica veins. Several barite veins intruded parallel or subparallel to the bedding plane of the chert.

At three sections of the chert/barite beds (Fig. 4), rock samples were collected from entire horizons without any absence. These three sections are called L2, L3, and L4. Sections L3 and L4 are located 2 m and 12 m from L2, respectively. The stratigraphies of these sections are shown in Fig. 6, and compiled as a standard stratigraphy of the chert/barite beds at Locality-3 in Fig. 7.

The fossil-bearing chert/barite beds are composed of 10 lithologically distinct layers: S1, S2, S3, S4, S5, S6, S7, S8, S9, and S10, from bottom to top (Figs. 5 and 7). The stratigraphies of all three sections are basically the same, except for a slight difference in thickness of some layers (Fig. 6).

3.2.1. Lithology

Lithologies of the greenstone and overlying sedimentary rocks of the 10 distinctive sedimentary layers are described below. In addition, lithologies of three types of veinlets (i.e., barite vein, barite-quartz vein, and chalcedony vein) and an intraformational breccia, are also described.

Greenstones are altered pillowed basaltic lavas indicating subaqueous eruption. The greenstones are strongly altered changing color into brown, although the ophitic texture of the original igneous rocks is preserved. Carbonate and chlorite dominate the secondary minerals without a Ca-Al silicate mineral assemblage. This suggests that a CO_2-rich hydrothermal fluid was responsible for the alteration of the pillow lava (Kitajima et al., 2001).

Breccia with cherty matrix (s1) is composed of 1 to 20 mm-wide greenish granules in a fine-grained silica and barite matrix (Fig. 8a). The greenish granules are mainly basaltic (Fig. 8b), show ophitic texture, are now composed of fine-grained silica, illite, and Ti-oxide, and in place have glass shards with vesicles (Fig. 8b). The matrix is transparent and is composed of fine-grained silica and barite. The matrix silica locally shows colloform texture, suggesting the replacement of former chalcedony.

Brown chert with pyrite (s2 and s4) is mainly composed of fine-grained (~ 1 μm) silica with scattered euhedral cubic pyrites 1 to 2 mm in diameter, which are partly replaced by hematite. The chert also contains trace amounts (less than 1 %) of fine-grained (~1μm) Ti-oxide and hexagonal pyrite suggesting former pyrrhotite (Fig. 8c). The chert rarely contains rhombic casts ~0.1 mm in diameter suggesting former carbonate. Hematite and barite occur as secondary minerals mainly along cracks. The chert has a flat lamination.

Gray chert (S3) is mainly composed of fine-grained silica and minor Fe-oxide. The gray chert includes a ~1cm-thick normal-grading arenaceous layer

(Fig. 8d), in which 0.1 mm to 1 mm volcaniclastics (?) are encompassed by a transparent silica and barite matrix.

Fossil-bearing light gray chert (s5) is mainly composed of fine-grained silica (95 %) with minor (<5 %) Ti-oxide, hematite, pyrite, and spinel ($(Cr, Al)_2(Fe, Zn)O_4$), which are all fine-grained (Figs. 8f and 8g). Some hematite replaces cubic pyrite suggesting that the hematite is secondary. The light gray chert also contains small amount of carbonaceous matter including microfossils (see below). The chert is massive and has no lamination (Fig. 8e).

Brown thinly laminated chert (s6) is composed of fine-grained silica (>90 %), hematite (~5 %) with minor Ti-oxide, pyrite, and spinel, which are all fine-grained (Fig. 9a). 0.5mm thick wavy laminations are partly developed.

Polymictic breccia (s7) is composed of 1 mm to 2 cm angular to subangular rubble surrounded by fine-grained silica, opaque minerals and barite matrix (Fig. 8c). Clastics consist of chert, barite and basaltic fragments (Fig. 9d). In contrast with other breccias, the matrix contains opaque minerals and is not transparent; this suggests that the matrix was silicified mud.

Alternating barite and silica (S8 and S10) is composed of thin (0.2 to 0.5 mm) barite and silica layers, forming 3 to 10 cm-wide stromatolite-like domes (Fig. 9b), several of which grow upward from the rubble of the underlying breccia (Fig. 9c). The barite and silica layer is partly composed of elongated white amorphous silica clasts scattered in a barite and silica matrix, where stromatolite-like domes are sparse.

Brown-and-light green banded chert (s9) consists of alternating bands of ~1 cm-thick flat brown and light green chert. Light green chert is mainly composed of fine-grained silica (>90 %) with chlorite and epidote. Brown layers are mainly composed of fine-grained silica (>95 %) with barite (~3 %), hematite (~1 %), and minor (<0.1 %) pyrite, spinel, and Ti-oxide, which are all fine-grained (~3 μm).

Chalcedony veins are transparent and composed of chalcedony, which is now replaced by fine-grained silica (~1μm), but has a colloform texture, and occasionally large quartz grains, 0.1-1 cm in diameter. The colloform texture grows toward the interior from the both walls. The typical width of the chalcedony veins are 10 to 50 μm and occasionally extends to 1-10cm (Figs. 8e, 10a, and 10c).

Barite veins are blue gray and are mainly composed of anhedral barite, 0.2 to 3 mm in diameter with fine-grained (~1μm) silica (Fig. 9e). The silica partly shows colloform texture, suggesting a replacement of former chalcedony. The width of the barite vein is 1 to 15 cm.

Barite-quartz veins are white and are composed of euhedral, relatively large barite, 0.1 to 5 cm in diameter and quartz, 50 to 500 μm in diameter. The barite is partly replaced by silica.

Intraformational breccia is composed of monomictic, poorly sorted, subangular to subrounded chert clasts (1 mm to 10 cm) within a barite/silica matrix (Figs 10b, 10c, and 10d). Each grain of the intraformational breccia has the same lithology as that of the chert intruded by the veins. The intraformational breccia occurs in the barite-silica veins. In contrast with the sedimentary breccia, the matrix of the intraformational breccia is composed of transparent silica and barite and not of silicified mud.

3.2.2. Correlation between beds and veins

Intrusive pattern of the chalcedony vein: Chalcedony veins mainly intruded parallel to the bedding and some vertically. Along the chalcedony veins, chert is partly broken to form an intraformational breccia with little displacement of fragments (Figs 10a and 10b). The chalcedony veins are usually cut by the barite veins, and some vertical chalcedony veins are concordant with the barite veins (Fig. 5 left).

Intrusive pattern of the barite veins: The barite veins intruded vertically or nearly parallel to the bedding of the chert (Fig. 5). At the roof and floor of the nearly horizontal barite veins, the vein barrettes clearly cut the lamination of the chert and horizontal, small chalcedony veins (Figs. 10a, 10b, and 10c). The horizontal barite veins usually intruded along the layer boundary (e.g., the boundary between s3 and s4; Fig. 5) and partly intruded a single bedded chert layer. Along the horizontal barite vein intruding a single bedded chert layer, the bedded chert is partly broken or brecciated to form an intraformational breccia (mentioned above). A vertical barite vein (80 cm in width) cross-cuts the layer s1 and probably s2 and s3 (left part of Fig. 5). The top of the vein is eroded and capped by the chert layer s4. This large barite vein is accompanied by chalcedony. The growth pattern of the barite and chalcedony is symmetrical to the central axis of the vein.

Intrusive pattern of the barite-quartz vein: The barite-quartz veins usually intrude subparallel to the bedding of the chert (Fig. 5), and cuts the formerly-mentioned chalcedony veins and barite veins. The width of the single barite-quartz vein changes from 2 cm to 1m. The upper left of Fig. 5 shows that the barite-quartz vein intruded along the fault with dips about 10° from the bedding plane. Layers s8 to s10 on the vein are displaced to the lower left in Fig. 5 by ~ 2 m, and folded in the trend of the displacement.

Fissure-filling chert structure: As shown in the middle of the left half of the Fig. 5, two fissure-filling structures occur. A brown pyrite-bearing chert (s4) filled fissures in the underlying chert beds and greenstone. The fissure-filling chert looks similar to the silica dikes, but they are different by the presence of laminations parallel to those of the adjacent chert beds. This chert partly includes chert fragments, 3 to 10 cm in diameter (left part of the Fig. 5). These observations indicate that the chert filled extensional cracks with wall rock fragments.

4. Carbonaceous filamentous microstructures

Newly-found filamentous microstructures occur in the light gray chert in the middle horizon of the bedded chert-barite unit at Locality-3. Sometimes, more than 20 filaments are enclosed in a gray chert clast in the breccia, but these are absent in their matrix (Fig. 10d). The filaments are concentrated in relatively small domains (~1 mm^2) in thin sections. These filaments are oriented randomly in chert and are not parallel to the bedding.

4.1. Descriptions

The filaments are morphologically subdivided into the following two types: Type-A and Type-B.

Type-A are segmented broad (4 to 16 μm; average 8.7 μm, n=10), unbranched filaments and are not ensheathed (Figs. 11a, 11b, and 11c). They are brown to black and have relatively smooth surfaces that are clearly different from inorganic angular surfaces of crystalline morphology. Each segment is cylindrical and a hemispherical terminal shape. This type of filament is composed of carbonaceous material and Ti-oxide (anatase).

Type-B are unbranched, tubular, broad filaments (7 to 20 μm; average 12.6 μm, n=17), that are not segmented (Figs. 11d and 11e). They are dark brown to black, and are composed of carbonaceous material and Ti-oxide (anatase). They have relatively rough surfaces, probably due to thermal maturation of carbonaceous material.

4.2. Interpretation

The newly-found filaments have carbonaceous compositions and are distinguishable from inorganic crystalline morphologies. They are similar in size and morphology to previously reported Archean fossil bacteria. The Type-A broad filaments are comparable to the *Archaeoscillatoriopsis maxima* and *A. grandis* reported by Schopf (1993) from the Warrawoona Group, and the Type-B to the *Siphonophycus antiquus*; reported by Awramik et al. (1983) from the same area. Hence, the filaments are probably classified into the same taxa previously reported as fossil-bacteria. The broad (especially >10 μm in diameter) septated filamentous morphology of the Type-A filament is also similar to that of several modern trichomic bacteria, such as osillatriacean cyanobacteria and beggiatoacean gliding bacteria (Buchanan and Gibbons, 1974). The Type-B filament has a tubular, non-septate unbranched morphology, and roughly resembles tubular sheaths of several modern bacteria, such as sheathed bacteria (e.g., *Clonothrix*) and cyano-bacteria (e.g., *Symploca*) (Buchanan and Gibbons, 1974).

5. Carbon isotopes

5.1. Methods

We selected a chert sample (96NPS90-95) containing probable carbonaceous microfossils for carbon isotopic measurements. 96NPS90-95 is a light gray bedded chert from Locality-1. The reduced carbon concentration of the light gray bedded chert is very low (less than 0.01 wt%; Ueno, 2002). Thus, separation and concentration of micron-scale carbonaceous matter were needed for the analysis.

Carbon isotopic measurements were performed by secondary ion mass spectrometry (SIMS) using a CAMECA ims1270 at Tokyo Institute of Technology. The rock sample was crushed into rock powder and dissolved with HF for 24 hours at room temperature. Acid-insoluble residues were mounted on a glass plate (6 mm x 6 mm) and Au-coated (~50 nm thickness).

Details of the SIMS analytical procedure are given in Ueno et al. (2001). Analytical reproducibility for $\delta^{13}C$ values, based on USGS24 graphite standards, is better than ±2 ‰.

5.2. Results

The results of the analyses are listed in Table 1 and are shown in Fig. 12. The separated carbonaceous matter from sample 96NP90-95 shows various morphologies (i.e., filamentous, flattened, ellipsoidal, and irregular-shaped, rough-surface carbonaceous matter). Their $\delta^{13}C$ values are –40.2 to –30.5 ‰. There is no clear correlation between their morphologies and the carbon isotopic compositions.

The carbon isotopic composition of sedimentary organic matter can be modified by several geological processes after deposition. However, the metamorphic grade of the North Pole area including the rocks studied here, is generally low (prehnite-pumpelleyite to lowermost greenschist facies; Dunlop and Buick, 1981; Kitajima et al., 2001). According to Ueno et al. (2001), the carbonaceous matter in the studied area became enriched by only a few permil in ^{13}C through the graphitization process. In addition, $\delta^{13}C$ values of carbonaceous matter in silica dikes were enriched in ^{13}C by ~3 ‰ during post-depositional alteration (Ueno, 2002). Hence, the measured $\delta^{13}C$ values of the carbonaceous matter reported here are regarded as the maxima of originally lower values.

6. Discussion

We will first discuss the depositional environment of the fossil-bearing chert/barite beds, then the isotopic composition of carbonaceous matter in the fossil-bearing chert bed together with the morphology of the filamentous microfossils. We will finally discuss physiological aspects of Early Archean microorganisms in the North Pole area.

6.1. Depositional environment of fossil-bearing chert

Here, we discuss the lithofacies of the fossil-bearing chert/barite beds at Locality-3 and further suggest that their deposition was closely related to hydrothermal activity in an extensional regime.

6.1.1. Lithofacies of fossil-bearing chert/barite beds

The fossil-bearing chert/barite beds in Locality-3 are composed of five lithofacies: 1. banded chert; 2. chert with fine-grained mafic clastics; 3. breccia with a cherty matrix; 4. polymictic breccia; and 5. alternating barite and silica.

Banded chert (s9) is mainly composed of silica and has no clastics. The flat banding consists of Fe-oxide-bearing brown layers and chlorite/epidote-bearing green layers. This appearance is similar to that of banded iron formation. The characteristics indicate direct precipitation of silica with or without Fe-oxide from silica-saturated brine.

Chert with fine-grained mafic clastics (s2-s6) are mainly composed of silica with fine-grained TiO_2, spinel, and hematite. The fine-grain size as well as the massive or parallel-lamination without any cross-lamination suggest that the fine-grained clastics were deposited sufficiently distant from a land mass and well below wave-base. Two possible origins of the silica are inferred. One is that the silica was directly precipitated from silica-saturated brine with the fine-grained mafic clastics, similar to the banded chert. The other is that the chert was originally deposited as mud and underwent post-depositional silicification. Some cherts with fine-grained mafic clastics have barite and carbonate pseudomorphs, which are replaced by fine-grained silica. These textures indicate post-depositional silicification of the sediment.

Breccia with cherty matrix (s1) is composed of basaltic fragments cemented by fine-grained silica and barite matrix. The transparent matrix is only composed of pure silica and barite and lacks sand or mud. This is distinct from the normal clastic sediments. The matrix silica partly shows colloform texture suggesting direct precipitation of silica probably from colloids. Such evidence indicates that the breccia was probably deposited in an environment where silica sinter developed.

Polymictic breccia (s7) is composed of basalt, chert, and barite fragments cemented by fine-grained silica and barite. The matrix also contains fine-grained opaque minerals, suggesting former mud. All the rock fragments are endemic to the chert/barite unit and are poorly sorted. This indicates that the clastics were derived from the same or adjacent basin as that of the chert/barite unit.

Alternating barite and silica (s8 and s10) show domal stratiform structure, which resembles stromatolite (Lowe, 1980; Walter et al., 1980). However, their biological origin are much debated (Grotzinger and Rothman, 1996; Lowe, 1994a). No microfossil-like structures or carbonaceous matter have been observed in this structure. The alternating barite and silica directly overlie polymictic breccia. The association with breccia and the domal structure is similar to that of barite mounds in this area (Nijman et al., 1999), which are directly connected with barite veins suggesting chemical precipitation from a hydrothermal fluid.

In summary, the fossil-bearing chert/barite beds are mainly composed of silica with or without mafic clastics. The lack of quartzo-feldspathic clastics indicates that the volcanism of the basin was mafic, not bimodal. Further, their generally fine-grain size, lack of coarse-grained terrigenous clastics, and their generally parallel-lamination or banding suggest that the fossil-bearing chert beds were deposited sufficiently distant from a land mass and well below the wave base (see also Kitajima et al., this volume for detailed discussion of the depositional depth of the chert-barite unit).

6.1.2. Hydrothermal activity

In pioneering studies, Groves et al. (1981) and Buick and Dunlop (1990) described silica-replaced textures of diagenetic carbonate and sulfate in the North Pole chert-barite unit. They suggested pervasive post-depositional silicification. Recent findings of direct connections of the silica dikes and barite veins with the chert-barite unit (Isozaki et al., 1997; Nijman et al., 1999; Ueno et al., 2001) indicate that the chert/barite deposition was synchronous with hydrothermal activity. Thus, the silicification may have taken place soon after deposition or during deposition of the chert-barite unit.

In the fossil-outcrop (Fig. 5), several generations of barite and chalcedony veins cut the chert/barite beds. Some barite veins penetrate the chert layers s1-s3 nearly parallel to the bedding surface (Fig. 3), but they do not cut the fissure-filling chert and s4. This indicates that some barite veins were formed before the deposition of the chert layer s4. Similarly, the vertical barite vein (Fig. 5 left) cuts the bedding surfaces of chert layers s1-s3, but is depositionally overlain by chert s4. These observations confirm that the formation of the silica dike and barite vein were synchronous with the deposition of the fossil-bearing chert/barite beds.

Some barite veins are accompanied by silica (Fig. 5 left). The alternation of barite and silica defines a symmetrical pattern along the vein axis (Fig. 9e). They partly show colloform texture grown from the hanging wall toward the center of the veins. These observations indicate that the barite and silica veins were precipitated from a silica- and barium-rich hydrothermal fluid, which filled the conduit. The fanning pattern of distribution of the barite veins (Fig. 2) suggests that the injections of barium-rich hydrothermal fluid started at depth and the barite was precipitated at a shallower level. The barite veins occur only in shallower depths, less than 200 m below the chert barite unit. The distribution suggests that the barite veins formed probably by the mixing between a reduced, high-temperature barium-rich hydrothermal fluid and relatively oxidized, low-temperature sea water.

Consequently, these lines of evidence suggest that the deposition of the fossil-bearing chert/barite beds was closely related to hydrothermal exhalative activity in an extensional regime. This indicates that the silica and barite were mainly derived from a silica- and barium-rich hydrothermal fluid.

6.2. Carbon isotopic signature and significance of filamentous microfossils

$\delta^{13}C$ values of kerogen in fossil-bearing chert vary from –40 to –31 ‰. These highly ^{13}C-depleted isotopic compositions strongly indicate the biogenic origin of the kerogen, because their values are too for inorganic carbon compounds. The $\delta^{13}C$ values of sedimentary carbonate from the same North Pole chert-barite unit is ~0 ‰ (Hayes et al., 1983), which is nearly equal to that of modern marine carbonate. Thus, the carbon isotopic fractionation between carbonate and kerogen is up to 30-40 ‰. It is unrealistic to attribute such a large fractionation to non-biological processes (Mojzsis et al., 1996; Schidlowski et al., 1983). In modern environments, such ^{13}C-depleted organic matter is produced essentially by autotrophic carbon fixation. In the fossil-bearing chert, carbonaceous matter occur matter occur as the filamentous microfossils. Thus, the filaments probably have similar carbon isotopic compositions. This is consistent with biogenicity of the filaments, which are morphologically similar to modern filamentous bacteria. Consequently, the significant ^{13}C-depletion of the carbonaceous matter clearly indicates that it was originally produced by biological carbon fixation.

Several known carbon fixation pathways utilized by autotrophic bacteria produce different degrees of carbon isotopic fractionation. The degree of the fractionation is controlled by many physico-chemical factors such as P, T, pCO_2, growth rate of the cell, and so on. However, the maximum fractionation can be experimentally determined, for example by growth experiment under sufficiently high-pCO_2 condition (e.g., Padue et al., 1976). Therefore, the $\delta^{13}C$ values of the carbonaceous matter in the fossil-bearing chert can constrain the carbon fixation pathway utilized by ancient autotrophic bacteria. Fig. 12B shows the maximum fractionation of extant autotrophic bacteria determined by growth experiments of previous investigators (Preuß et al., 1989; Sirevåg et al., 1977; Holo and Sirevåg, 1986; Menedez et al., 1999; Padue et al., 1976). Large fractionation up to 40 ‰ could be attained by autotrophs utilizing the Calvin cycle or the reductive acetyl CoA pathway. On the other hand, such a large fractionation up to ~40 ‰ is not produced via the reductive citric acid cycle (Preuß et al., 1989; Sirevåg et al., 1977) or via the 3-hydroxypropionate cycle (Holo and Sirevåg, 1986; Menendez et al., 1999) unless CO_2 as a carbon source was not extraordinary enriched in ^{12}C. In addition, cyanobacteria such as *Oscillatoria. williamsii, Microcoleus chthonoplastes, Schizothrix calcicola* and *Synechococcus lividus* (Fig. 12; Padue et al., 1976) cannot produce such a large fractionation despite their utilization of the Calvin cycle. This is probably due to the different isotope effects by several rubisco isoenzymes (Goericke et al., 1994; Guy et al., 1993).

Among extant filamentous bacteria, almost broad filaments, more than 3.5 μm in width, are actually cyanobacteria (Schopf, 1993). The size and morphology of oscillatoriacean cyanobacteria are quite similar to some Early Archean filamentous microfossils from the Marble Bar area (Schopf, 1993) and North Pole area (this study; Awramik et al., 1983; Schopf and Walter, 1983). The significant ^{13}C-depletions are apparently inconsistent with morphological similarity of the filaments to cyanobacteria. The inconsistency indicates that we should be careful to evaluate the physiological aspects of fossil bacteria only from their morphology. It is noted that some extant trichomic filamentous bacteria >3.5 μm wide can fractionate carbon isotopic composition up to 40 ‰ via the Calvin cycle (e.g., beggiatoacean filamentous bacteria). The broad filaments are possibly chemoautotrophic bacteria utilizing the Calvin cycle.

6.3. Early Archean microbial community in a seafloor hydrothermal system

The North Pole chert-barite unit contains considerable amounts of ^{13}C-depleted carbonaceous matter (average 0.05 wt%; $\delta^{13}C$ = -37 to –29 ‰; Hayes et al., 1983; Strauss et al., 1992; Ueno, 2002) as well as carbonaceous microfossils (Awramik et al., 1983; Schopf and Walter, 1983; Ueno et al., 2001). In spite of the difficulties of recognition of the morphological microfossils because of their poor preservation and simple morphology, this evidence strongly suggests that the autotrophic organisms were active during the deposition of the chert-barite unit.

In contrast to previous depositional models of a simple evaporitic shallow marine setting, the results of this study clearly indicate that the deposition of the fossil-bearing chert was closely associated with hydrothermal activity. Therefore, a microbial community including autotrophic bacteria probably existed in the Early Archean seafloor hydrothermal system.

Furthermore, black silica dikes, which filled sub-seafloor fractures at the time of chert-barite deposition, contain abundant ^{13}C-depleted carbonaceous matter (average 0.2 wt%, $\delta^{13}C$ = –38 to –30 ‰, n = 33; Ueno, 2002) and filamentous probable microfossils with a highly ^{13}C-depleted isotopic composition (Ueno et al., 2001). Fig. 13 shows the distribution of the kerogen-bearing silica dikes. Among the studied 601 silica dike specimens, 587 (98 %) contain kerogen. Thus, the ^{13}C-depleted carbonaceous matter is widely distributed in the chert/barite beds as well as in the silica dikes propagated beneath the Archean seafloor. This confirms the existence of Early Archean organisms in seafloor hydrothermal systems. Moreover, this evidence strongly indicates that their habitat spread into the sub-seafloor hydrothermal system.

The silica dikes are mainly composed of fine-grained silica (>90 %) and their sulfide-content is low (typically <5 %). These characteristics are comparable to those of modern low temperature (100 to 150 ˚C) hydrothermal vent mineralization, but dissimilar to high temperature (200 to 350 ˚C) massive sulfide deposits (Hannington et al., 1995). Thus, the silica dike probably formed at a temperature less than 200 ˚C. The temperature of a hydrothermal fluid, in which Early Archean bacteria lived, has never been directly determined, although the sub-seafloor microbial community may have included thermophilic and hyperthermophilic bacteria. Modern hyperthermophiles can grow in water up to about 120 ˚C (Stetter, 1998). We note that non-thermophilic organisms could also have been included in the community, because the hydrothermal venting was probably intermittent.

Physiological aspects of the microbes in Early Archean hydrothermal systems are still poorly known. However, significant ^{13}C-depletion of carbonaceous matter indicates that the community included autotrophic organisms. A possible energy source of the autotrophs is light (photosynthesis) or inorganic compounds (chemosynthesis). However, the photosynthetic activity is uncertain, because the fossil-bearing chert/barite beds at Loc.-3 generally show massive or parallel-lamination and have no cross-lamination, suggesting deposition below wave base (< 80 m). The euphotic zone of the modern ocean is about 80 m below the surface. Moreover, Kitajima et al. (2001) recognized mineral zonation caused by sea-floor metamorphism of basalt below the chert-barite unit and estimated that the hydrothermal fluid circulation started from phase-separation of water at ~350°C. This indicats that the depositional depth of the chert-barite unit was deeper than ~1500 m. Thus, a deeper origin of the chert-barite unit is also possible and likely. It is problematic that photosynthesis could have been active at the depth of the chert/barite deposition.

On the other hand, it is highly plausible that chemoautotrophs were included in the hydrothermal microbial community, because the redox gradient of the hydrothermal system could have provided various electron donors and acceptors (Fig. 14). Available electron donors were probably H_2S, CH_4, H_2, Fe^{2+}, etc. Micro-Raman analyses (Kitajima et al., this volume) indicate that fluid inclusions in vein barite contain CO_2, H_2S, and CH_4. Available electron acceptors were probably CO_2, SO_4^{2-}, etc. Therefore, methanogenesis ($CO_2 + 4H_2 = CH_4 + 2H_2O$) and sulfate reduction ($SO_4^{2-} + 2CH_2O = S^{2-} + 2CO_2 + 2H_2O$ or $SO_4^{2-} + 4H_2 = S^{2-} + 4H_2O$) are possible energy yielding processes. Ueno et al. (2001) reported carbonaceous filaments with high ^{13}C-depletion ($\delta^{13}C$ = –42 to –32 ‰) in silica dikes. Both their morphology and isotopic fractionation are comparable to some methanogens (e.g. *Methanobacterium thermoautotrophicum*). This may support the existence of methanogen in the Early Archean hydrothermal system. Shen et al. (2001) suggested the existence of sulfate-reducer based on more than 18 ‰ sulfur isotopic fractionation between sulfate and sulfide in the North Pole chert-barite unit.

Another candidate for available electron acceptor is molecular oxygen. Modern hydrothermal vent communities include aerobic chemosynthesizers, which depend on O_2 derived from photosynthesis at the sea surface (Jannasch, 1995). However, oxygen fugacity of Early Archean sea water is generally considered to have been very low (Kasting, 1993; Lowe, 1994b), although it is poorly known and difficult to estimate (detailed discussions are given in Holland, 1999; Ohmoto, 1997). Thus, it is uncertain whether aerobic chemosynthesis such as sulfide oxidation, methane oxidation, and iron oxidation were active or not in the

Archean seafloor hydrothermal system.

In summary, the microbial community in the Early Archean hydrothermal system probably included chemosynthetic primary producers. One of the possible differences from modern hydrothermal vent communities is absence of aerobic chemosynthesizers.

6.4. Proposed model for the Early Archean seafloor hydrothermal ecosystem

Based on the above discussions, Fig. 14 summarizes the inferred depositional environment of the North Pole chert-barite unit. The deduced general sedimentation process of the fossil-bearing chert/barite bed is as follows:

1. Pillowed basalt was erupted on the seafloor.
2. The pillowed basalt was partly brecciated by extensional fault activity. Silica-rich and/or barium-rich hydrothermal fluids with the basalt detritus were emitted through the extension fractures.
3. At the bottom of the chert bed, emitted basaltic debris accumulated and was cemented by the silica (and barite) into silica sinter.
4. Bedded chert was chemically precipitated from the silica-rich hydrothermal fluid with or without fine-grained mafic clastics, which may also have been emitted through the hydrothermal vent.
5. Bedded barite was occasionally precipitated by the mixing of the barium-rich hydrothermal fluid and relatively oxidized low-temperature seawater.
6. Silica and/or barite filled the fractures, which had been the conduits of the hydrothermal fluid, to form silica dikes or barite veins.
7. The sequence of extensional fault activity, deposition of chert/barite, formation of silica/barite vein, and silicification of sediments was repeated several times.

Emitted hydrothermal fluids on the seafloor provided various electron donors and acceptors to bacterial communities including chemosynthetic primary producers. Numerous extensional fractures were developed in the uppermost 1000 m of the oceanic crust, where the hydrothermal fluids were intermittently circulated. The bacterial communities including thermophiles/hyperthermophile also inhabited the sub-seafloor hydrothermal system.

7. Conclusions

Microfossil and carbon isotope analyses combined with geological and petrological analyses of fossil-bearing chert-barite beds provided the following conclusions.

1. Carbonaceous filamentous microstructures, newly found from bedded chert in ca. 3.5 Ga North Pole chert-barite unit, are morphologically similar to trichomic filamentous bacteria and bacterial sheaths, and are classified into previously known taxa of Archean microfossils.
2. $\delta^{13}C$ values of carbonaceous matter from the fossil-bearing chert range from –40 to –31 ‰. The highly ^{13}C-depleted carbonaceous matter was probably derived from biological carbon fixation via the Calvin cycle or the reductive acetyl-CoA pathway, but could not have been produced by cyanobacteria.
3. Fossil-bearing chert/barite beds are mainly composed of fine-grained silica and barite with or without mafic clastics, and lack quartzo-feldspathic coarse-grained clastics. They generally show parallel-lamination, are partly massive and lack cross-lamination. These lines of evidence suggest that the fossil-bearing chert was deposited sufficiently distant from a land mass and probably well below wave base.
4. Cross-cutting relationships between fossil-bearing chert/barite beds and silica and barite veins suggest that the chert/barite deposition was synchronous with the vein formation in an extensional regime. This confirms that the deposition of fossil-bearing chert/barite beds was closely related to hydrothermal exhalative activity. The silicification of the sediments probably took place soon after their deposition and during the deposition of the chert-barite unit.
5. Huge amounts of ^{13}C-depleted carbonaceous matter are concentrated in the silica dikes, which were developed in the uppermost 1000 m of the Early Archean oceanic crust. This indicates that the originally biogenic organic carbon was condensed in the sub-seafloor fractures.
6. These observations suggest that the seafloor and sub-seafloor hydrothermal system was the habitat of Early Archean life. The Early Archean microbial community in the hydrothermal system was probably supported by chemosynthetic primary producers.

Acknowledgements

We thank M. Terabayashi, Y. Kato, T. Kabashima, K. Okamoto and K. Kitajima for great assistance in the field and the field collaboration with A. Thorne and A. H. Hickman was helpful and greatly appreciated. We also thank an anonymous reviewer for helpful comments. This research was supported by the Ministry of Culture and Education of Japan (International Scientific Research Program; field research nos. 06041038 and 08041102 and Intensified Study Area Program, no. 259, 1995-1997).

References

Awramik, S.M., Schopf, J.W., and Walter, M.R., 1983, Filamentous fossil bacteria from the Archean of Western Australia: Precambrian Research, v. 20, p. 357-374.

Awramik, S.M., Schopf, J.W., and Walter, M.R., 1988, Carbonaceous filaments from North Pole, Western Australia: Are they fossil bacteria in Archaean stromatolites? A discussion: Precambrian Research, v. 39, p. 303-309.

Blake, T.S., 1993, Late Archean crustal extension, sedimentary basin formation, flood basalt volcanism and continental rifting: the Nullagine and Mount Jope Supersequences, Western Australia: Precambrian Research, v. 60, p. 185-241.

Buchanan, R.E., and Gibbons, N.E., 1974, Bergey's Manual of Determinative Bacteriology, 8th edition: Baltimore, Williams and Wilkins, 1246 p.

Buick, R., 1984, Carbonaceous filaments from North Pole, Western Australia: Are they fossil bacteria in Archaean stromatolites?: Precambrian Research, v. 24, p. 157-172.

Buick, R., 1988, Carbonaceous filaments from North Pole, Western Australia: Are they fossil bacteria in Archaean stromatolites? A reply: Precambrian Research, v. 39, p. 311-317.

Buick, R., and Dunlop, J.S.R., 1990, Evaporitic sediments of Early Archean age from the Warrawoona Group, North Pole, Western Australia: Sedimentology, v. 37, p. 247-277.

Dunlop, J.S.R., and Buick, R., 1981, Archaean epiclastic sediments derived from mafic volcanics, North Pole, Pilbara Block, Western Australia, in Glover, J.E., and Groves, D.I., eds., Archaean Geology, Second International Symposium, Volume 7: Perth, Geological Society of Australia, Special Publication, p. 225-233.

Fuchs, G., Thauer, R., Ziegler, H., and Stichler, W., 1979, Carbon isotope fractionation by *Methanobacterium thermoautotrophicum*: Archives of Microbiology, v. 120, p. 135-139.

Goericke, R., Montoya, J.P., and Fry, B., 1994, Physiology of isotopic fractionation in algae and cyanobacteria, in Lajtha, K., and Michener, R.H., eds., Stable Isotopes in Ecology and Environmental Science: Oxford, Blackwell, p. 187-221.

Grotzinger, J.P., and Rothman, D.H., 1996, An abiotic model for stromatolite morphogenesis: Nature, v. 383, p. 423-425.

Groves, D.I., Dunlop, J.S.R., and Buick, R., 1981, An early habitat of life: Scientific American, v. 245, p. 56-65.

Guy, R.D., Fogel, M.L., and Berry, J.A., 1993, Photosynthetic fractionation of the stable isotopes of oxygen and carbon: Plant Physiology, v. 101, p. 37-47.

Hannington, M.D., Jonasson, I.R., Herzig, P.M., and Petersen, S., 1995, Physical and chemical processes of seafloor mineralization at mid-ocean Ridges, Seafloor Hydrothermal Systems: Physical, Chemical, Biological, and Geological Interactions, American Geophysical Union, p. 115-157.

Hayes, J.M., Kaplan, I.R., and Wedeking, K.W., 1983, Precambrian organic geochemistry, preservation of the record, in Schopf, J.W., ed., Earth's Earliest Biosphere: Princeton, NJ, Princeton University Press, p. 93-134.

Holland, H.D., 1999, When did the Earth's atmosphere become oxic? A reply: Geochemical News, v. 100, p. 20-22.

Holo, H., and Sirevåg, R., 1986, Autotrophic growth and CO_2 fixation of *Chloroflexus aurantiacus*: Archives of Microbiology, v. 145, p. 173-180.

Isozaki, Y., Kabashima, T., Ueno, Y., Kitajima, K., Maruyama, S., Kato, Y., and Terabayashi, M., 1997, Early Archean mid-oceanic ridge rocks and early life in the Pilbara Craton, W. Australia: EOS, v. 78, p. 399.

Isozaki, Y., Ueno, Y., Kitajima, K., Kabashima, T., and Maruyama, S., 1998, Early Archean mid-oceanic ridge sediments and the oldest bacteria from the Pilbara craton, W. Australia: The Geological Society of America, Abstracts with Programs, v. 30, p. A98.

Jannasch, H.W., 1995, Microbial interactions with hydrothermal fluids, Seafloor Hydrothermal Systems: Physical, Chemical, Biological, and Geological Interactions, American Geophysical Union, p. 273-296.

Kasting, J.F., 1993, Earth's early atmosphere: Science, v. 259, p. 920-926.

Kitajima, K., Maruyama, S., Utsunomiya, S., and Liou, J.G., 2001, Seafloor hydrothermal alteration at Archean mid-ocean ridge: Journal of Metamorphic Geology, v. 19, p. 583-600.

Lowe, D.R., 1980, Stromatolites 3,400-Myr old from the Archean of Western Australia: Nature, v. 284, p. 441-442.

Lowe, D.R., 1994a, Abiological origin of described stromatolites older than 3.2 Ga: Geology, v. 22, p. 387-390.

Lowe, D.R., 1994b, Early environments: constraints and opportunities for early evolution, *in* Bengston, S., ed., Early Life on Earth: New York, Columbia

University Press, p. 24-35.

Menendez, C., Bauer, Z., Huber, H., Gad'on, N., Stetter, K.O., and Fuchs, G., 1999, Presence of acetyl coenzyme A (CoA) carboxylase and propionyl-CoA carboxylase in autotrophic Crenarchaeota and indication for operation of a 3-hydroxypropionate cycle in autotrophic carbon fixation: Journal of Bacteriology, v. 181, p. 1088-1098.

Mojzsis, S.J., Arrhenius, G., McKeegan, K.D., Harrison, T.M., Nutman, A.P., and Friend, C.R.L., 1996, Evidence for life on Earth before 3,800 million years ago: Nature, v. 385, p. 55-59.

Mook, W. G., Bommerson, J. C., and Staverman, W. H., 1974, Carbon isotope fractionation between dissolved bicarbonate and gaseous carbon dioxide. Earth and Planetary Science Letters, v. 22, p. 169-176.

Nijman, W., de Bruijne, K.H., and Valkering, M.E., 1999, Growth fault control of Early Archaean cherts, barite mounds and chert-barite veins, North Pole Dome, Eastern Pilbara, Western Australia: Precambrian Research, v. 95, p. 247-274.

Ohmoto, H., 1997, When did the Earth's atmosphere become oxic?: Geochemical News, v. 93, p. 12-27.

Padue, J.W., Scalan, R.S., Van Baalen, C., and Parker, P.L., 1976, Maximum carbon isotope fractionation in photosynthesis by blue-green algae and a green alga: Geochimica et Cosmochimica Acta, v. 40, p. 309-312.

Preuß, A., Schauder, R., Fuchs, G., and Stichler, W., 1989, Carbon isotope fractionation by autotrophic bacteria with three different CO_2 fixation pathways: Zeitschrift für Naturforschung, v. 44c, p. 397-402.

Ruby, E.G., Jannasch, W., and Deuser, W.G., 1987, Fractionation of stable carbon isotopes during chemoautotrophic growth of sulfur-oxidizing bacteria: Applied and Environmental Microbiology, v. 53, p. 1940-1943.

Schidlowski, M., 2001, Carbon isotopes as biogeochemical recorders of life over 3.8 Ga of Earth history: evolution of a concept: Precambrian Research, v. 106, p. 117-134.

Schidlowski, M., Hayes, J.M., and Kaplan, I.R., 1983, Isotopic inferences of ancient biochemistries: carbon, sulfur, hydrogen, and nitrogen, in Schopf, J.W., ed., Earth's Earliest Biosphere: Princeton, NJ, Princeton University Press, p.

149-186.

Schopf, J.W., 1993, Microfossils of the Early Archean Apex Chert: New Evidence of the Antiquity of Life: Science, v. 260, p. 640-646.

Schopf, J.W. and Walter, M.R., 1983, Archean microfossils: New evidence of ancient microbes, in Schopf, J.W., ed., Earth's Earliest Biosphere: Princeton, NJ, Princeton University Press, p. 214-239.

Shen, Y., Buick, R., and Canfield, D.E., 2001, Isotopic evidence for microbial sulphate reduction in the early Archaean era: Nature, v. 410, p. 77-81.

Sirevåg, R., Buchanan, B.B., Berry, J.A., and Troughton, J.H., 1977, Mechanisms of CO_2 fixation in bacterial photosynthesis studied by the carbon isotope fractionation technique: Archives of Microbiology, v. 112, p. 35-38.

Stetter, K.O., 1998, Hyperthermophiles and their possible role as ancestors of modern life, in Brack, A., ed., The Molecular Origins of Life: New York, Cambridge University Press, p. 315-335.

Strauss, H., Des Marais, D.J., Hayes, J.M., and Summons, R.E., 1992, The carbon-isotopic record, in Schopf, J.W., and Klein, C., eds., The Proterozoic Biosphere: A Multidisciplinary Study: Cambridge, Cambridge University Press, p. 117-127

Thorpe, R.I., Hickman, A.H., Davis, D.W., Mortensen, J.K., and Trendall, A.F., 1992, U-Pb zircon geochronology of Archean felsic units in the Marble Bar region, Pilbara Craton, Western Australia: Precambrian Research, v. 56, p. 169-189.

Ueno, Y., Isozaki, Y., Yurimoto, H., and Maruyama, S., 2001, Carbon isotopic signatures of individual Archean microfossils (?) from Western Australia: International Geology Review, v. 43, p. 196-212.

Ueno, Y., Yurimoto, H., Yoshioka, H., Komiya, T., and Maruyama, S., 2002, Ion microprobe analysis of graphite from ca. 3.8 Ga metasediments, Isua supracrustal belt, West Greenland: Relationship between metamorphism and carbon isotopic composition: Geochimica et Cosmochimica Acta, in press.

Ueno, Y., 2002, Diversity of Earth's Earliest Life: Geology, Paleontology and Carbon Isotope Geochemistry of the Early to Middle Archean Fossil Record, Doctor Thesis, Tokyo Institute of Technology, 206 p.

Van Kranendonk, M., Hickman, A.H., Williams, I.S. and Nijman, W., 2001. Archaean geology of the East Pilbara Granite-Greenstone Terrane, Western Australia - a field guide. Geological Survey of Western Australia, record 2001/9, 134 p.

Walter, M.R., Buick, R., and Dunlop, J.S.R., 1980, Stromatolites 3,400-3,500 Myr old from the North Pole area, Western Australia: Nature, v. 284, p. 443-445. Cambridge University Press, p. 117-127.

Figure captions

Fig. 1 Simplified lithologic map of the North Pole area (modified after Isozaki et al., 1997). Numbers 1 and 2 indicate Localities- 1 and –2 of Ueno et al. (2001), respectively. Number 3 indicates Locality-3 (this study). The letters A and B indicate previously reported microfossil localities, corresponding to locality A and locality B of Awramik et al. (1983).

Fig. 2 Geologic map of the northern part of the North Pole area. Geological studies of specific outcrops (Locality-3) are described in detail.

Fig. 3 Stratigraphy of the nine tectonic slices.

Fig. 4 Lithologic sketch map and geologic profiles of Locality-3.

Fig. 5 A sketch of the fossil-bearing outcrop at Locality-3.

Fig. 6 Stratigraphy of the fossil-bearing chert/barite beds in sections L2, L3, and L4 at Locality-3.

Fig. 7 Generalized stratigraphy and nature of the fossil-bearing chert/barite beds at Locality-3. Compilation of the stratigraphies at sections L2, L3, and L4.

Fig. 8 a) Vertical cut-surface of breccia with cherty matrix. b) Photomicrograph under transmitted light of breccia with a cherty matrix. Dark parts are basalt fragments and grass-shards. The matrix (light) is composed of pure fine-grained silica. c) Back-scattered electron image of brown chert, which is composed of fine-grained silica (black) with TiO_2 (gray) and Fe-oxide (white). Some Fe-oxide replaced hexagonal pyrrhotite and rhombic carbonate. d) Arenaceous layer of the gray chert. Photomicrograph shows sand-size volcaniclastic clasts. e) Vertical cut-surface of fossil-bearing light gray chert. f) and g) Photomicrograph of light gray chert showing massive and fine-grained nature.

Fig. 9 a) Photomicrograph of brown thinly laminated chert. Parallel lamination is composed of alternating silica-rich layers and hematite-rich layers. b) Outcrop of the stromatolite-like barite and silica. Hammer is 30 cm long. c) Vertical cut-surface of polymictic breccia. d) Photomicrograph of silicified basalt fragment in the polymictic breccia, showing remains of ophitic texture. e) Outcrop of the barite vein (Fig. 5 left) with silica (white). Scale is 40 cm long.

Fig. 10 Barite vein with brecciated chert clasts. a) Vertical cut-surface of contact between light gray chert and layer-parallel barite vein (bottom). b) Vertical cut-surface of intraformational breccia. Photograph shows the light gray chert (bottom) and the brecciated gray chert surrounded by barite matrix. c) Sketch of the barite vein and intraformational breccia. d) Photomicrograph under transmitted light of light gray chert clasts. Arrows indicate carbonaceous filaments.

Fig. 11 Carbonaceous filaments from the light gray bedded chert at Locality-3. Optical photomicrographs of thin sections show Type-A (a and b) and Type-B (d and e) broad filaments. Figure c shows the schematic reconstruction of Figure b. Arrows in b indicate segmented parts suggesting former cells. Figures a and b are photomontages of two different focal depths. Scale bar shows 20 μm for all figures.

Fig. 12 a) *Upper column*: Carbon isotopic compositions of isolated kerogen (diamond) and carbonate (circle) in bedded chert and silica dikes. Filled symbol: Ueno (2002). Open symbol: Hayes et al. (1983). *Lower column*: Carbon isotopic composition of isolated carbonaceous matter from the fossil-bearing chert in Locality-3 (this study). b) Observed maximum carbon isotope fractionations in four different carbon fixation pathways by modern autotrophic bacteria. Filled circles show recalculated $\delta^{13}C$ values for autotrophs assuming their use of atmospheric CO_2 ($\delta^{13}C$ = –8 ‰), which is in equilibrium with carbonate ($\delta^{13}C$ = 0 ‰) at 25 °C (Mook et al., 1974). Sources of data for carbon isotope discrimination are as follows: a, Preuß et al. (1989); b, Fuchs et al. (1979); c, Ruby et al. (1987); d, Sirevåg et al.

(1977); e, Padue et al. (1976); and f, Holo and Sirevåg (1986).

Fig. 13 Distribution of kerogen-bearing silica dikes in the North Pole area.

Fig. 14 A schematic model for the depositional environment of the fossil-bearing chert/barite beds in an Early Archean hydrothermal system.

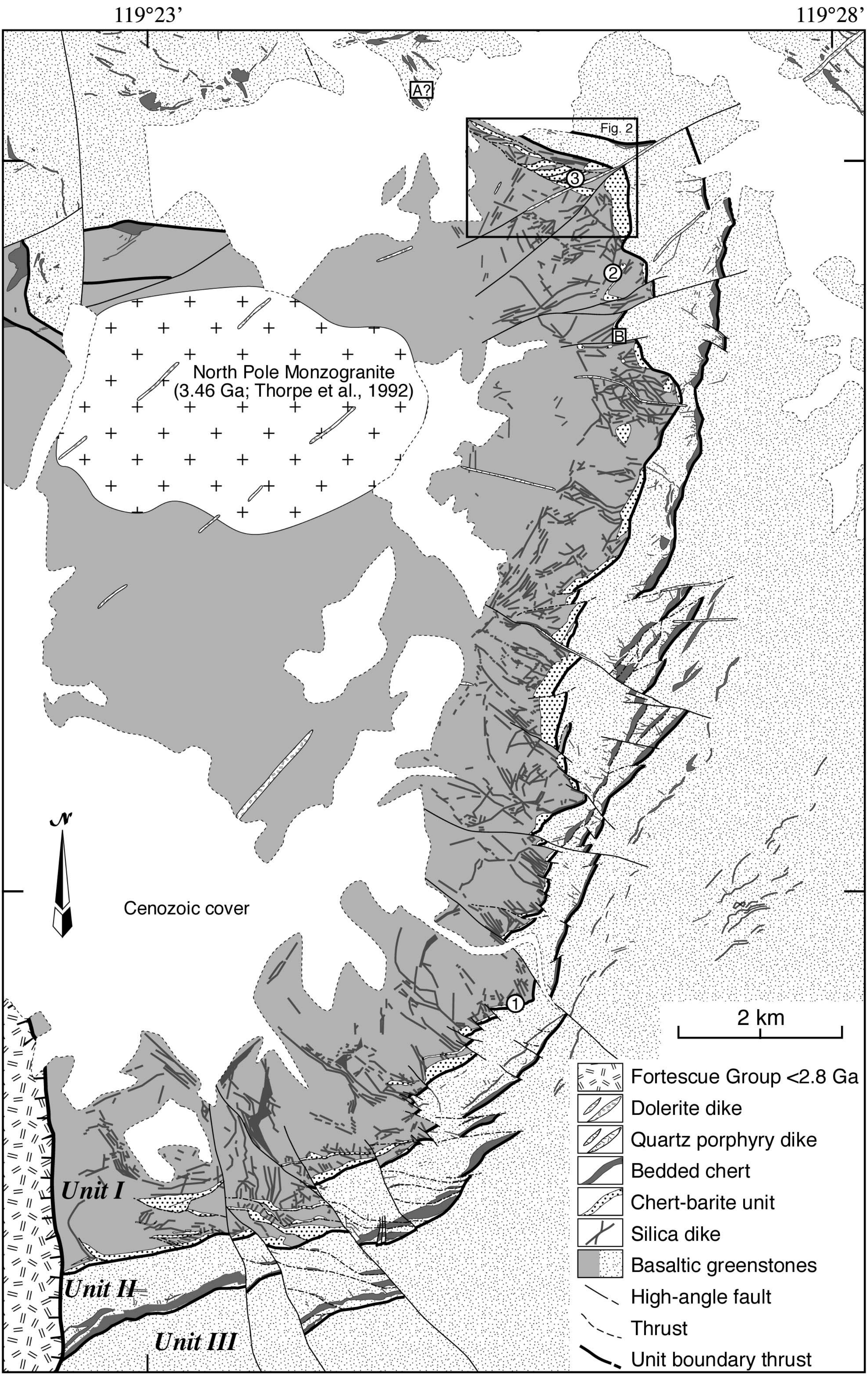

Ueno et al. Fig. 1

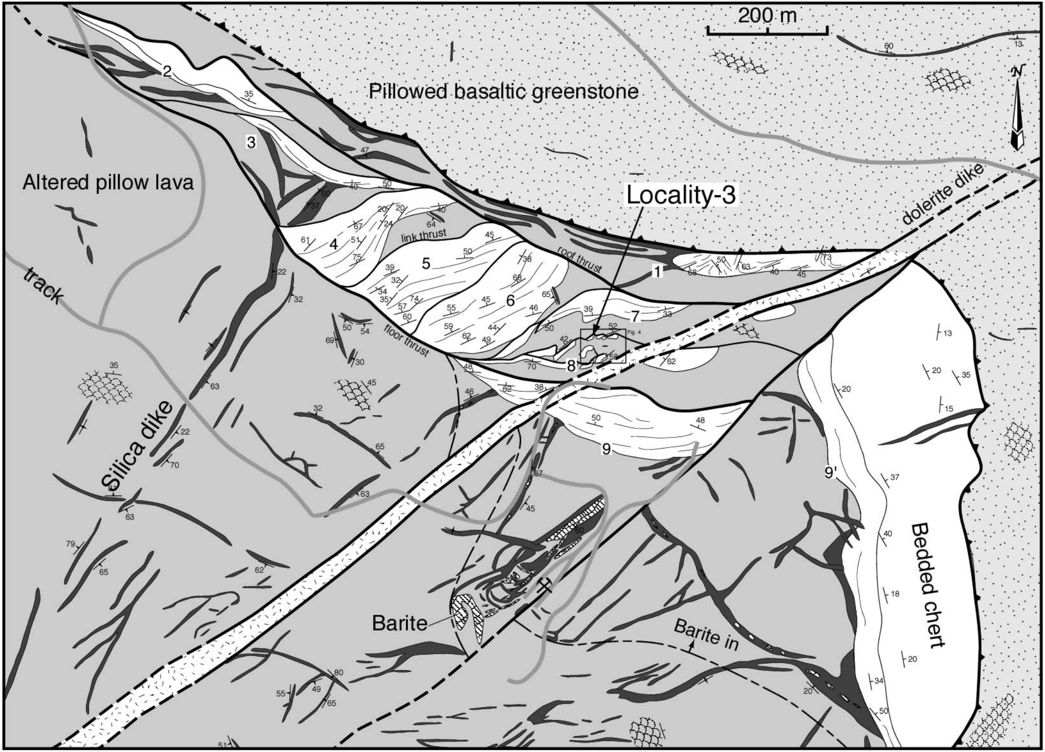

Ueno et al. Fig. 2

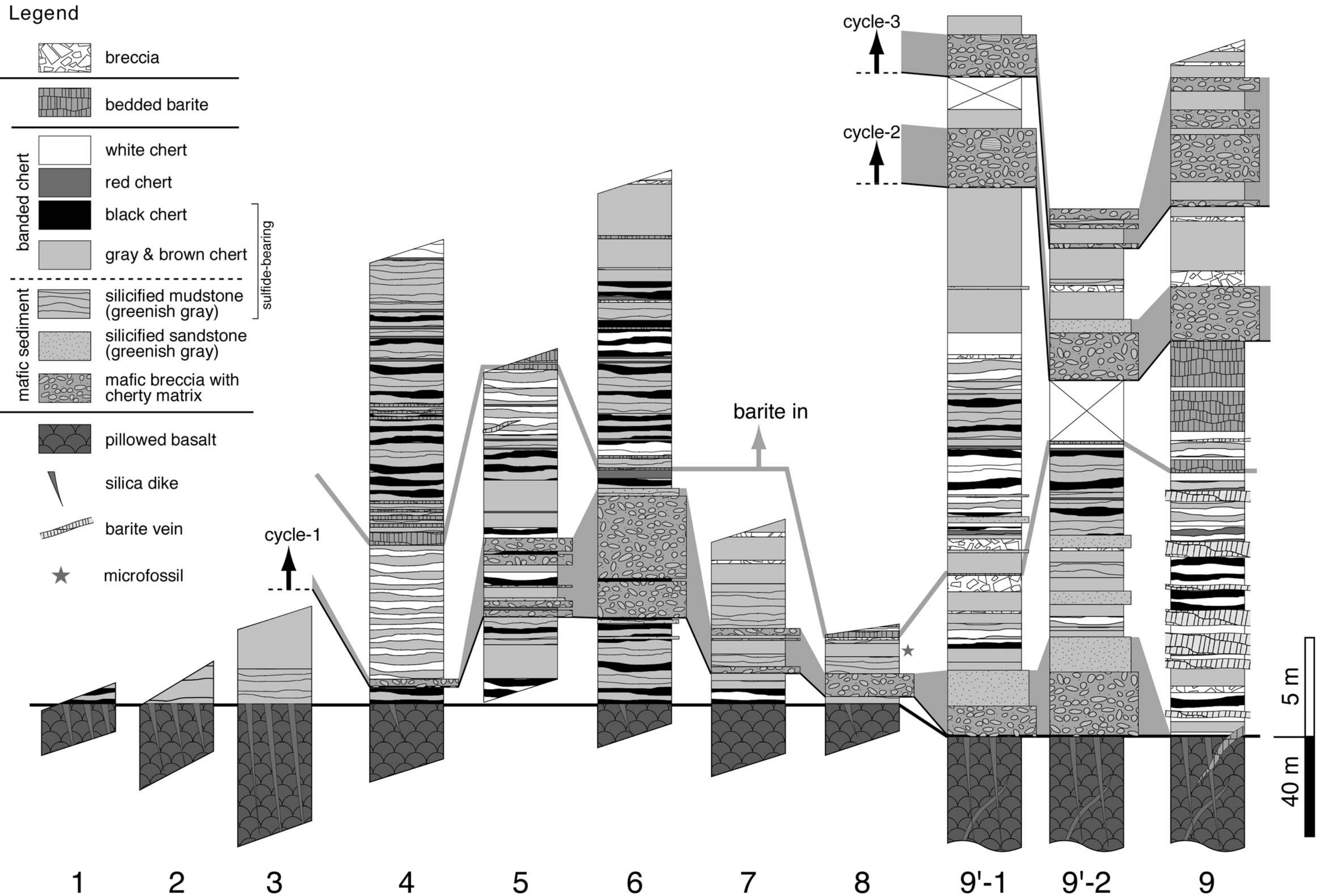

Ueno et al. Fig. 3

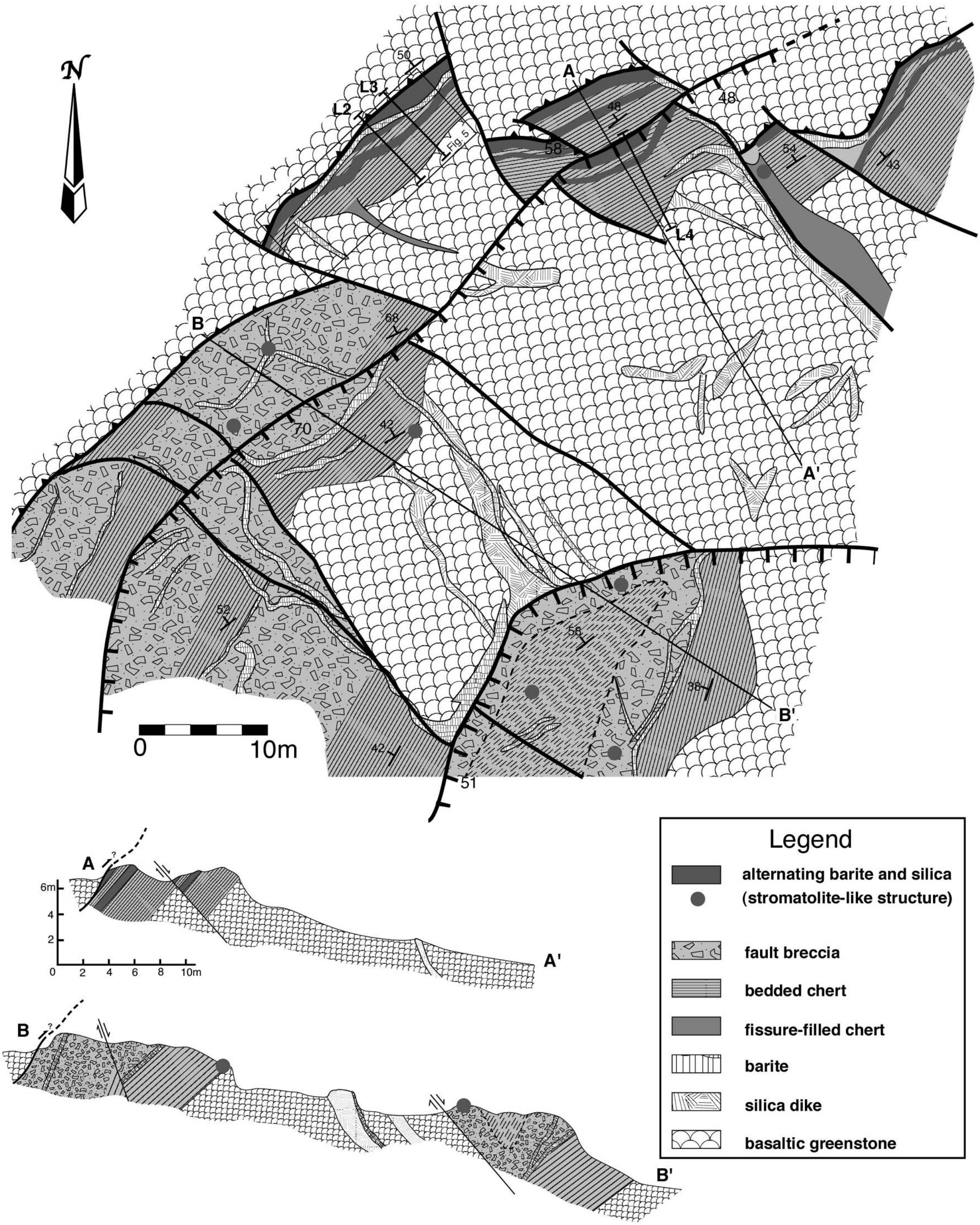

Ueno et al. Fig. 4

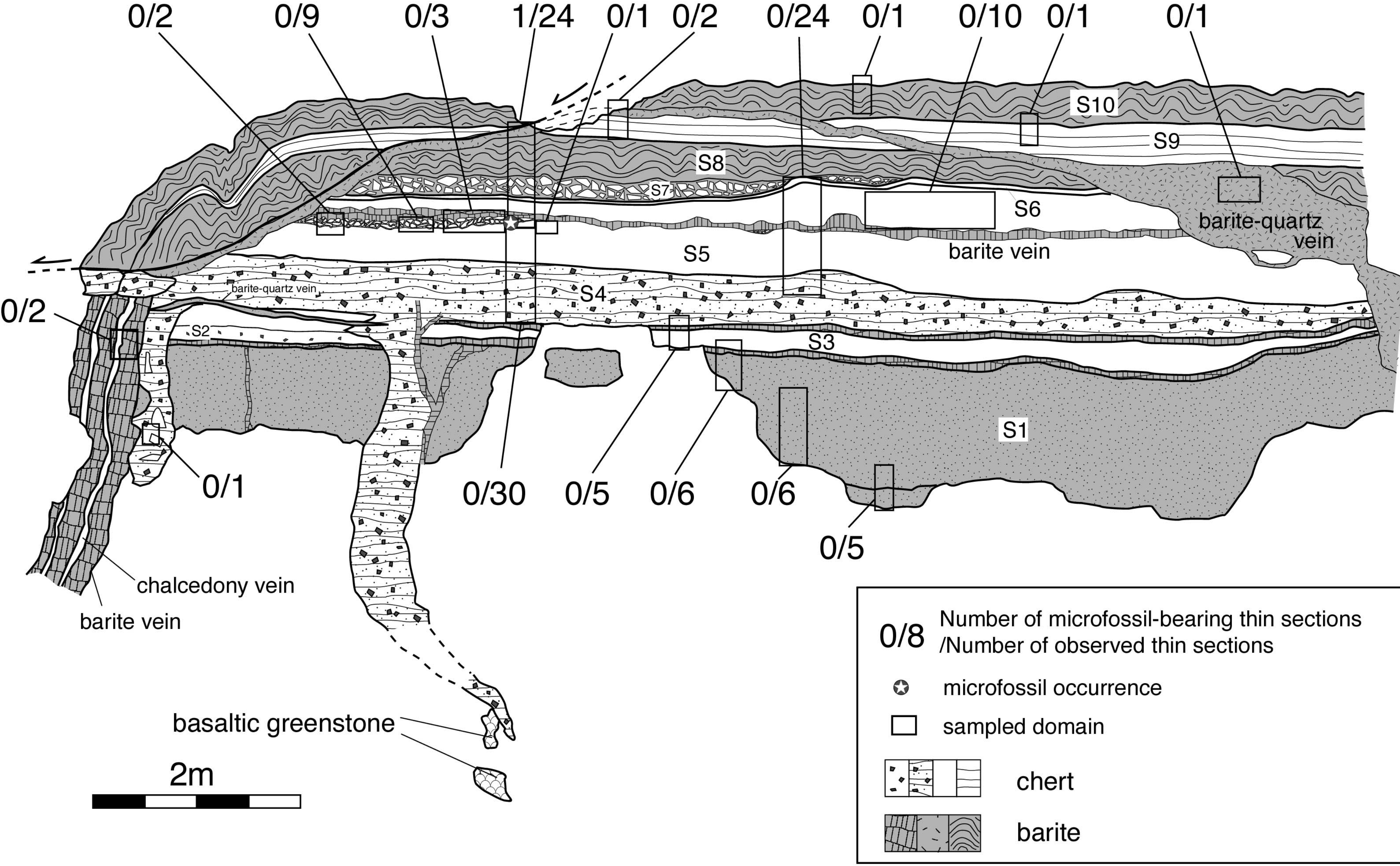

Ueno et al. Fig. 5

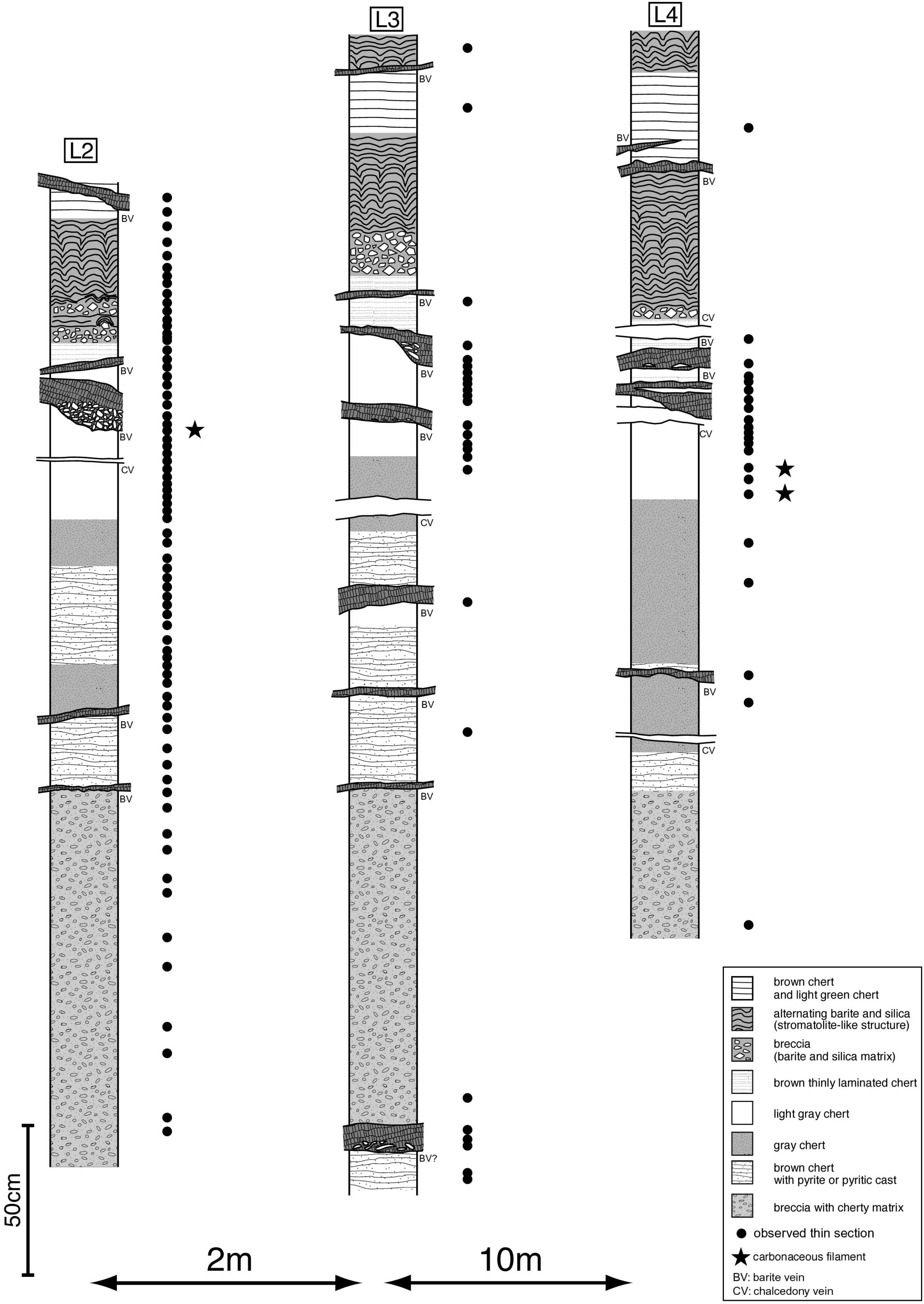

Ueno et al. Fig. 6

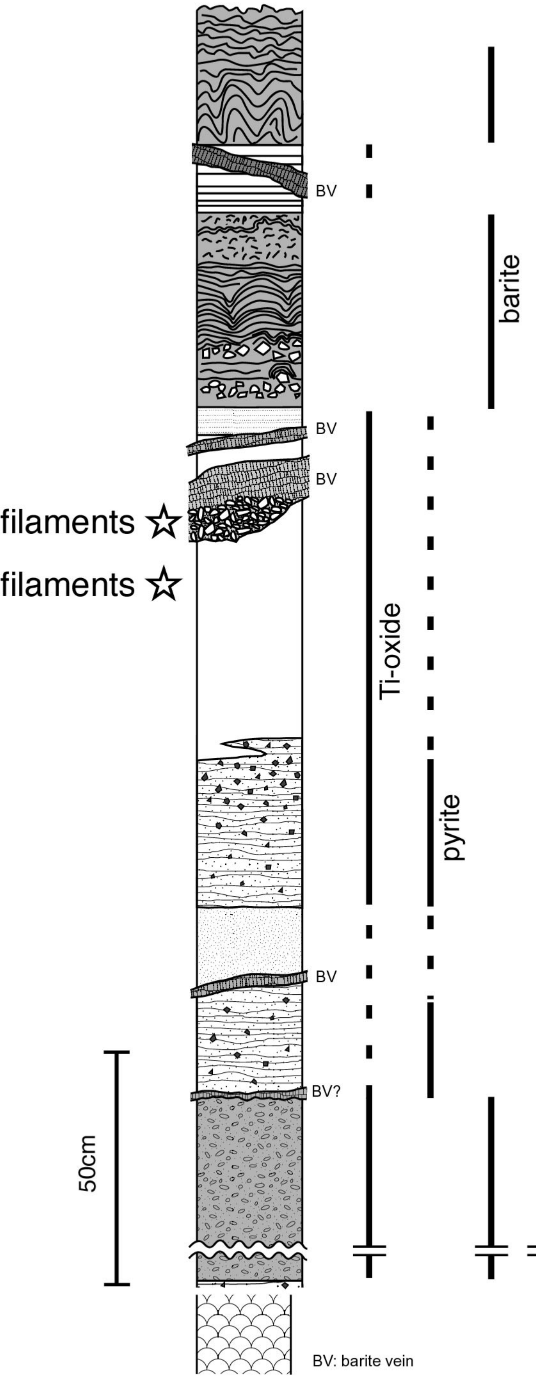

Unit	Sample	Lithology		clastics: basalt fragment	clastics: accretionary lapilli	clastics: chert fragment	clastics: barite fragment	clastics: fine-grained TiO_2	clastics: spinel ($(Fe, Zn)(Cr, Al)_2O_4$)	clastics: fine-grained zircon	matrix: silica	matrix: barite	euhedral minerals: pyrite	euhedral minerals: carbonate	euhedral minerals: epidote	euhedral minerals: chlorite	secondary: hematite	secondary: barite
D	S10	alternating barite and silica (stromatolite-like structure)		–	–	–	–	–	–	–	○	○	–	–	–	–	○	–
D	S9	brown-and-light green bandded chert	brown	–	–	–	–	△	△	–	◎	–	–	–	–	–	○	△
D	S9	brown-and-light green bandded chert	green	–	–	–	–	–	–	–	◎	–	–	△	△	△	△	△
D	S8	barite and silica / alternating barite and silica (stromatolite-like structure)		–	–	–	–	–	–	–	○	○	–	–	–	–	○	–
D	S7	polymictic breccia		○	–	○	○	–	–	–	○	○	–	–	–	–	○	–
C	S6	brown thinly laminated chert		–	–	–	–	○	△	△	◎	–	△	–	–	–	○	△
C	S5	light gray chert breccia / light gray chert		–	–	–	–	○	△	–	◎	–	△	△ ?	–	–	△	△
B	S4	brown chert with pyrite		–	–	–	–	○	–	–	◎	–	○	△ ?	–	–	○	–
B	S3	gray chert		–	–	–	–	△	–	–	◎	–	△	–	–	–	△	△
B	S2	brown chert with pyrite		–	–	–	–	△	–	–	◎	–	○	–	–	–	○	–
A	S1	breccia with cherty matrix		◎	○	–	–	○	–	–	○	○	–	–	–	△ ?	○	–

pillowed basaltic greenstone

◎: >80% ○: 1~80% △: <1%

Ueno et al. Fig. 7

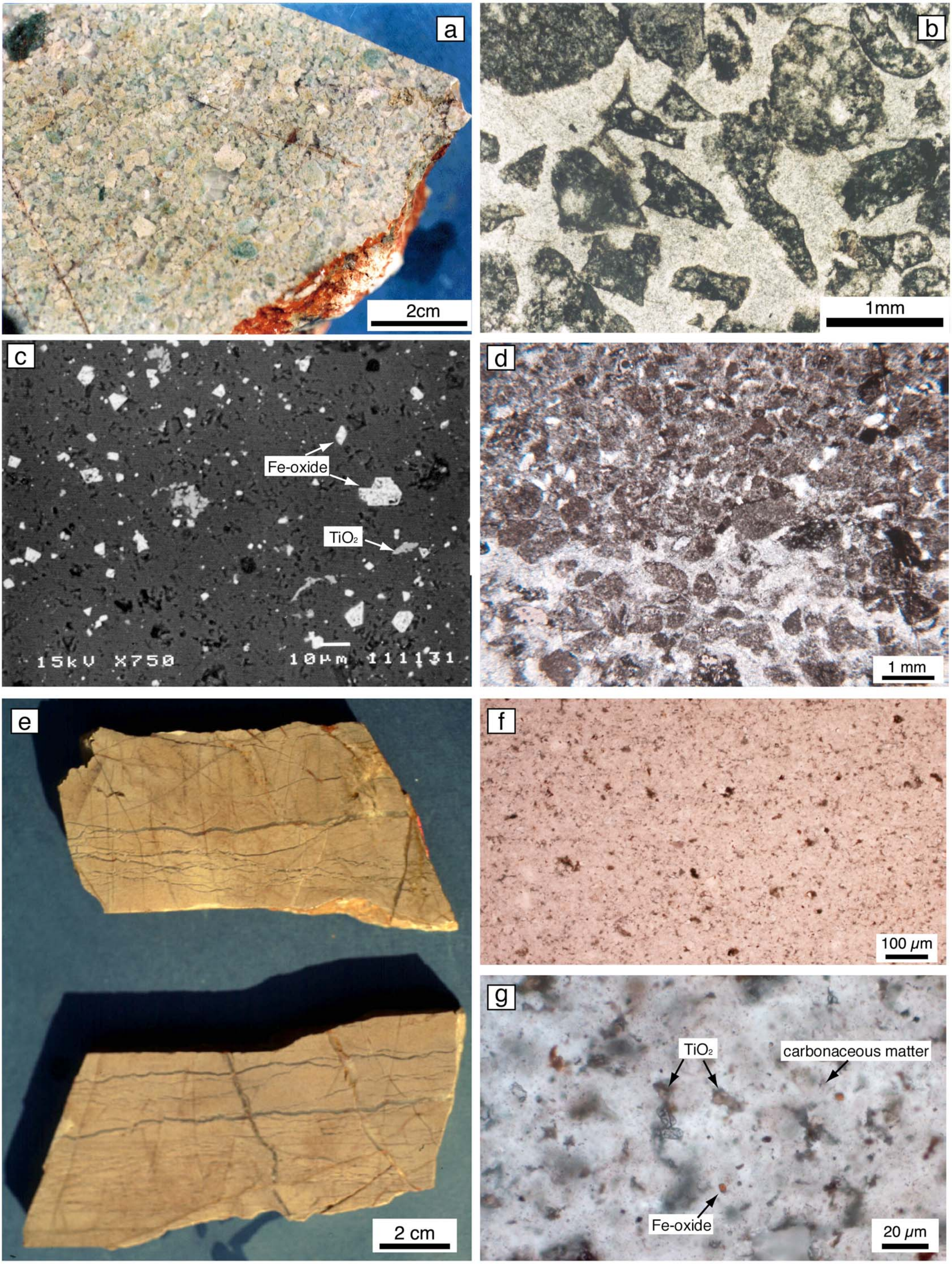

Ueno et al. Fig. 8

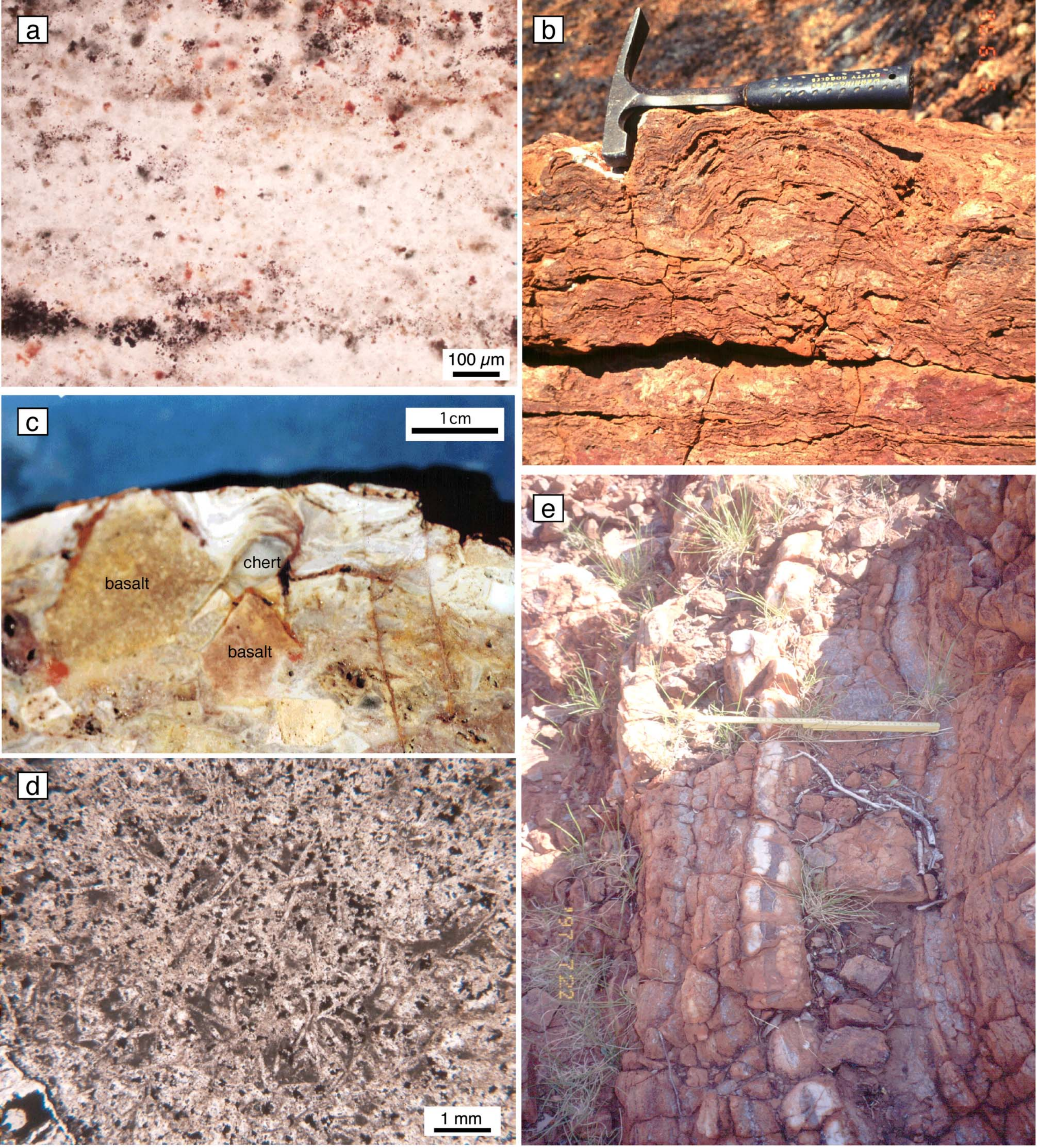

Ueno et al. Fig. 9

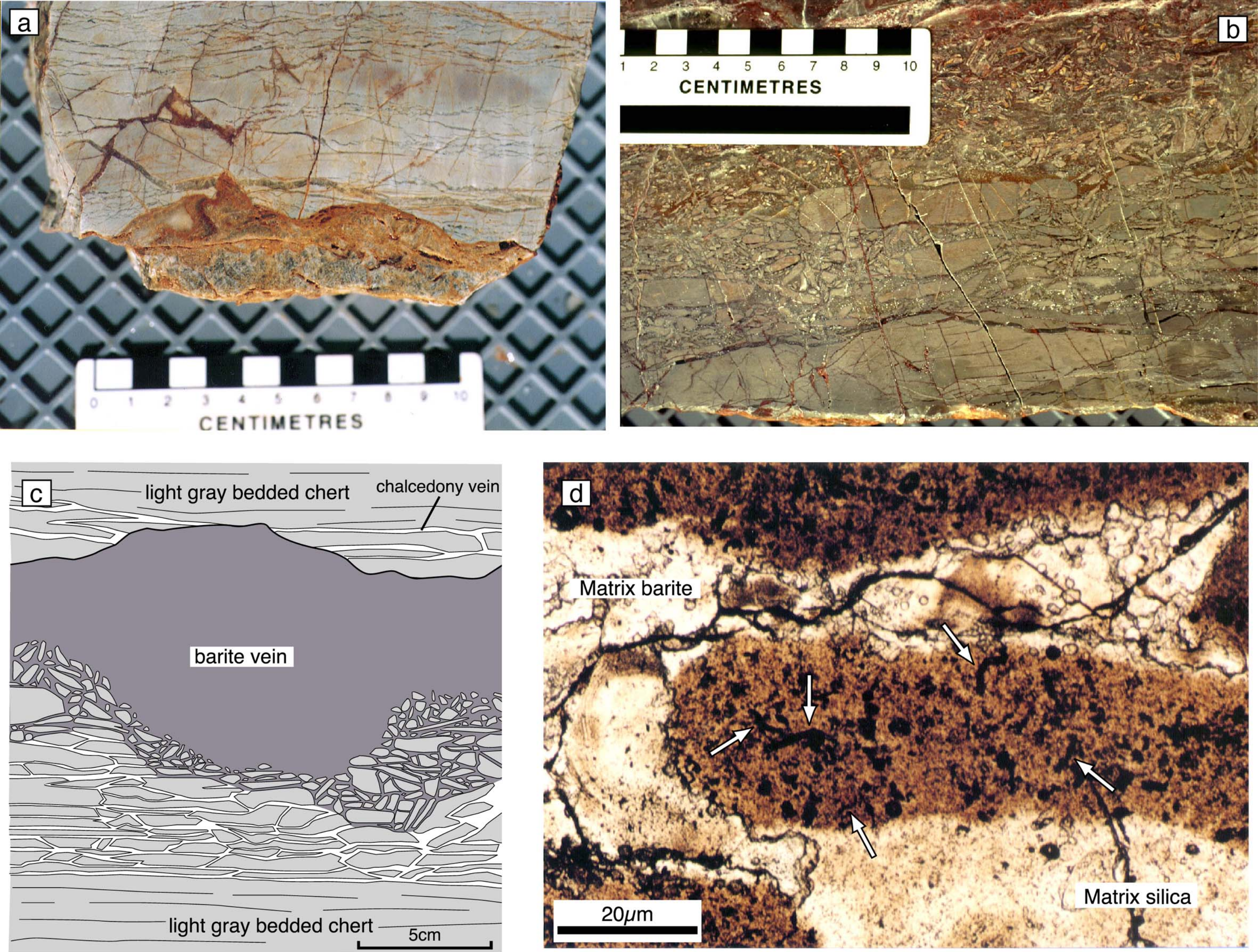

Ueno et al. Fig. 10

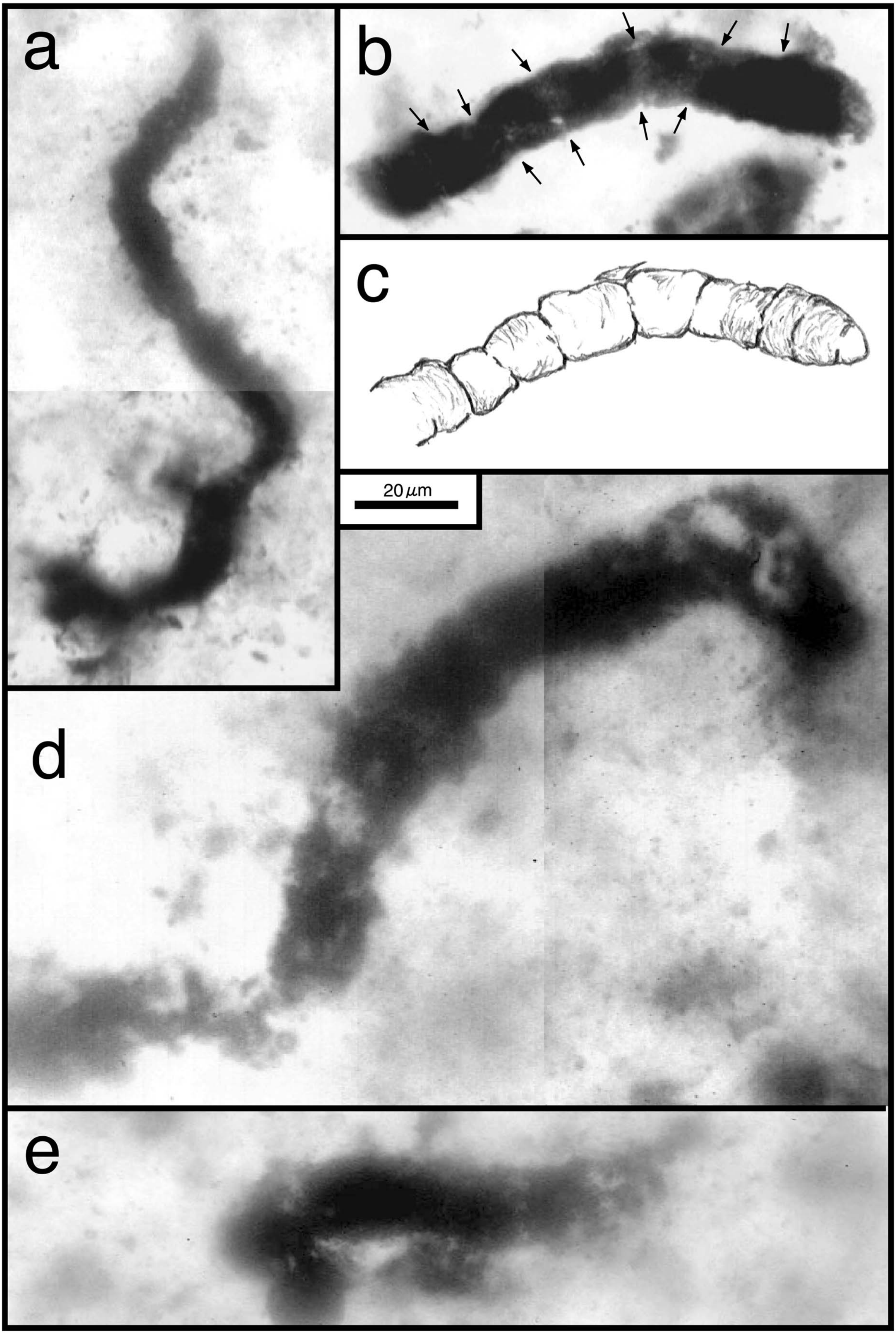

Ueno et al. Fig. 11

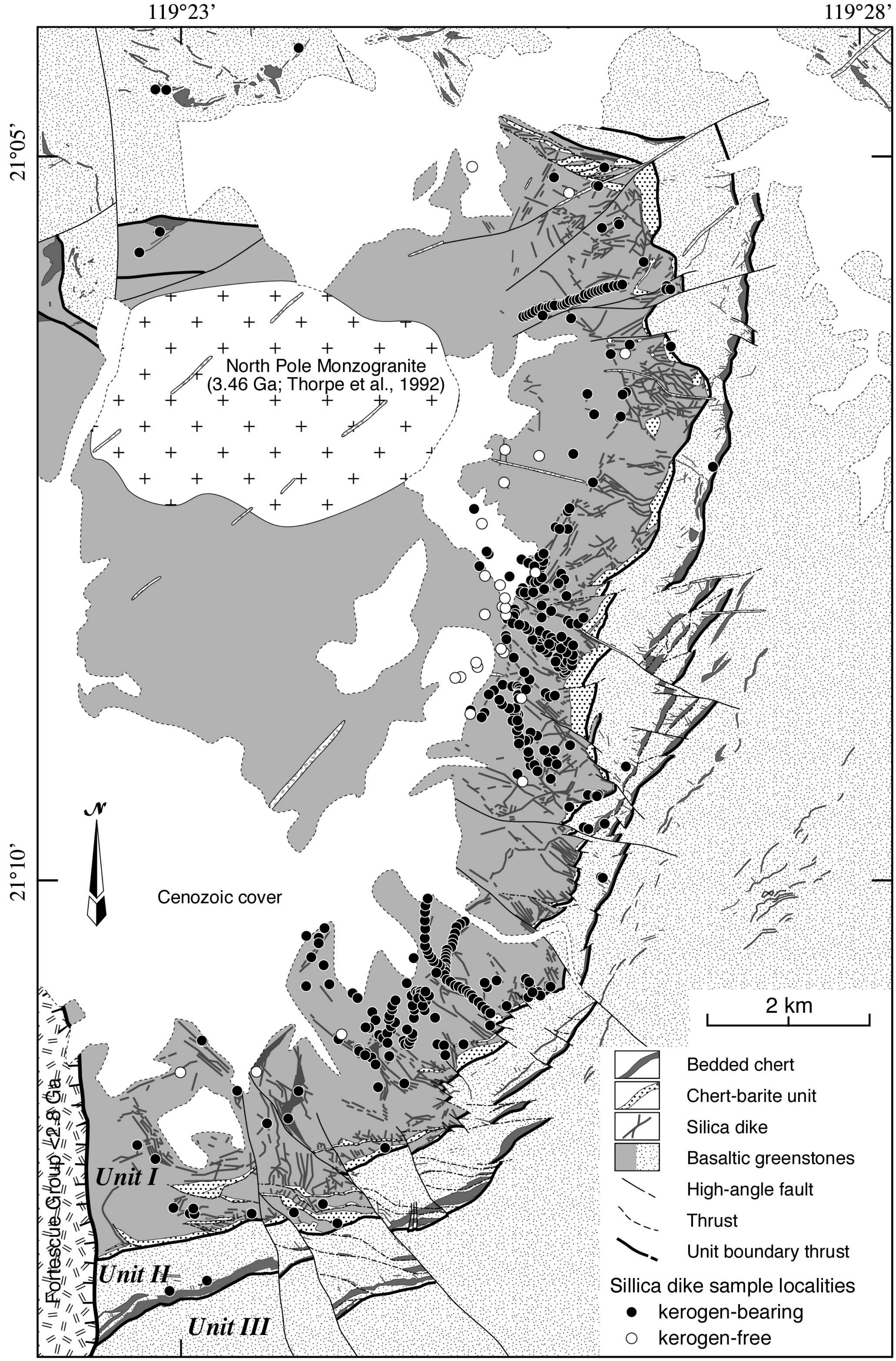

Ueno et al. Fig. 13

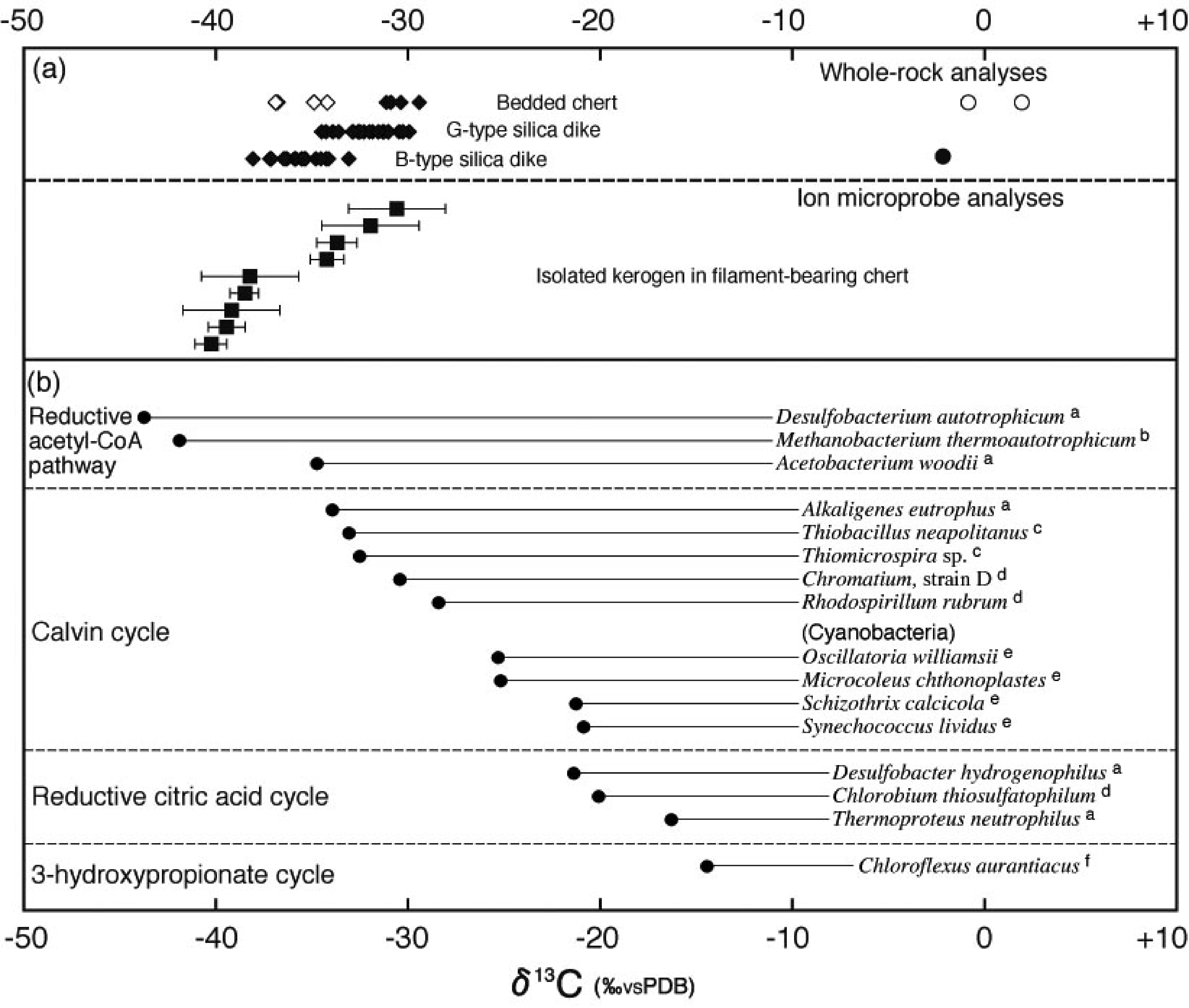

Ueno et al. Fig. 12

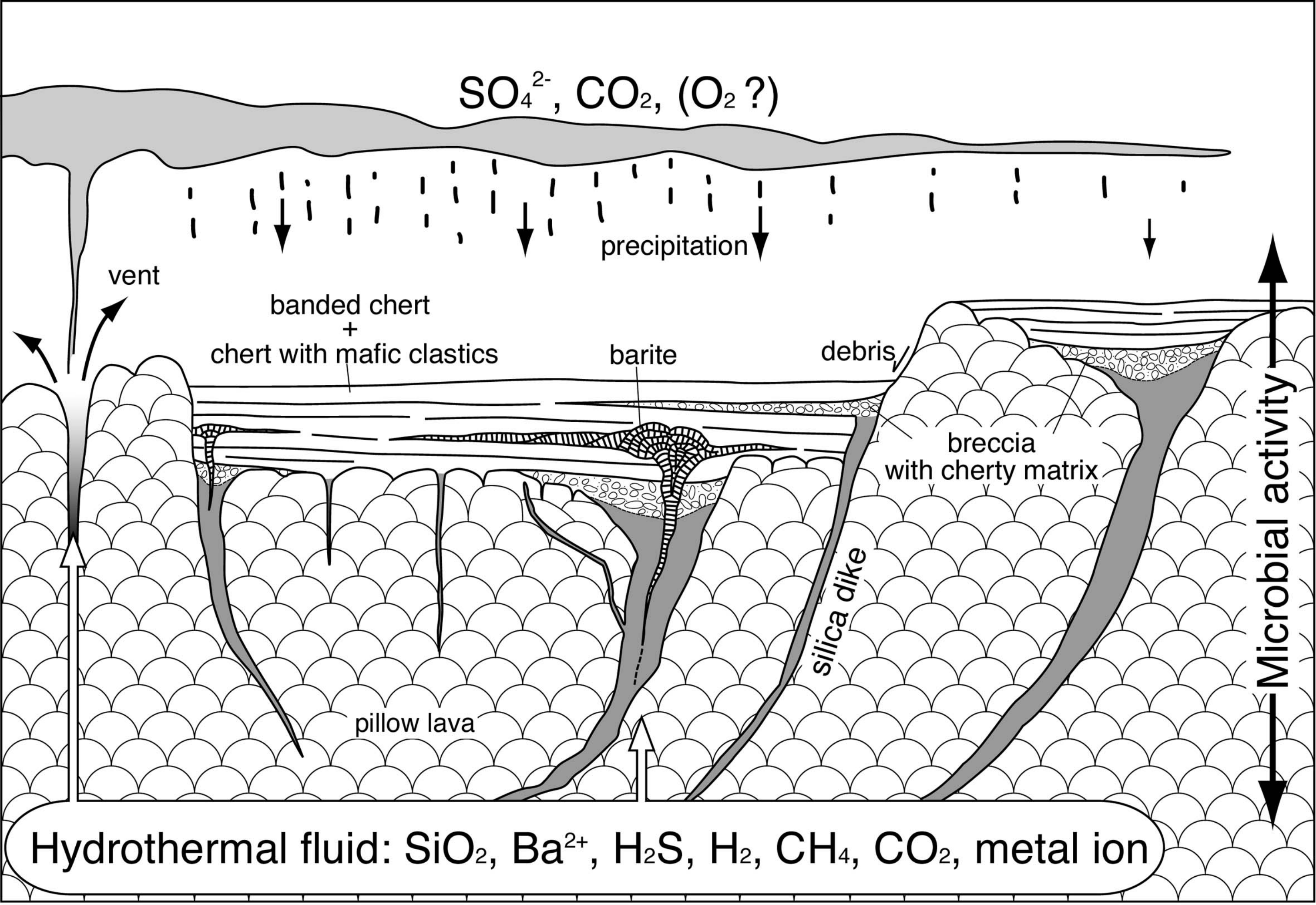

Ueno et al. Fig. 14